



A unifying concept of coccolithophore sensitivity to changing carbonate chemistry embedded in an ecological framework



Lennart Thomas Bach^{*}, Ulf Riebesell, Magdalena A. Gutowska¹, Luisa Federwisch², Kai Georg Schulz³

Biological Oceanography, GEOMAR Helmholtz Centre for Ocean Research Kiel, 24105 Kiel, Germany

ARTICLE INFO

Article history:

Received 25 October 2014

Received in revised form 20 April 2015

Accepted 20 April 2015

Available online 25 April 2015

ABSTRACT

Coccolithophores are a group of unicellular phytoplankton species whose ability to calcify has a profound influence on biogeochemical element cycling. Calcification rates are controlled by a large variety of biotic and abiotic factors. Among these factors, carbonate chemistry has gained considerable attention during the last years as coccolithophores have been identified to be particularly sensitive to ocean acidification. Despite intense research in this area, a general concept harmonizing the numerous and sometimes (seemingly) contradictory responses of coccolithophores to changing carbonate chemistry is still lacking to date. Here, we present the “substrate–inhibitor concept” which describes the dependence of calcification rates on carbonate chemistry speciation. It is based on observations that calcification rate scales positively with bicarbonate (HCO_3^-), the primary substrate for calcification, and carbon dioxide (CO_2), which can limit cell growth, whereas it is inhibited by protons (H^+). This concept was implemented in a model equation, tested against experimental data, and then applied to understand and reconcile the diverging responses of coccolithophore calcification rates to ocean acidification obtained in culture experiments. Furthermore, we (i) discuss how other important calcification-influencing factors (e.g. temperature and light) could be implemented in our concept and (ii) embed it in Hutchinson’s niche theory, thereby providing a framework for how carbonate chemistry-induced changes in calcification rates could be linked with changing coccolithophore abundance in the oceans. Our results suggest that the projected increase of H^+ in the near future (next couple of thousand years), paralleled by only a minor increase of inorganic carbon substrate, could impede calcification rates if coccolithophores are unable to fully adapt. However, if calcium carbonate (CaCO_3) sediment dissolution and terrestrial weathering begin to increase the oceans’ HCO_3^- and decrease its H^+ concentrations in the far future (10–100 kyears), coccolithophores could find themselves in carbonate chemistry conditions which may be more favorable for calcification than they were before the Anthropocene.

© 2015 The Authors. Published by Elsevier Ltd. This is an open access article under the CC BY license (<http://creativecommons.org/licenses/by/4.0/>).

Introduction

Coccolithophores, a group of marine phytoplankton, are among the most important CaCO_3 producers on our planet and an integral part of the marine carbon cycle. They contribute about 1–10% to marine primary production and about 50% to pelagic CaCO_3 deposition in sediments (Broecker and Clark, 2009; Poulton et al., 2007).

Calcification of coccolithophores feeds back on the climate system by (i) affecting the Earth’s albedo, (ii) decreasing CO_2 uptake capacity of the oceans via the reduction of total alkalinity, and (iii) enhancing carbon sequestration to depth by providing ballast material which accelerates sinking velocities of organic particles (Armstrong et al., 2002; Frankignoulle et al., 1994; Tyrrell et al., 1999). Thus, changes in the amount of CaCO_3 precipitated by coccolithophores can significantly impact global carbon cycling (Riebesell et al., 2009).

Increasing amounts of anthropogenic CO_2 currently accumulating in the ocean are severely perturbing the oceans’ carbonate system – a process termed ocean acidification. Consequences are a substantial decrease of carbonate ion (CO_3^{2-}) concentration, a minor increase of $[\text{HCO}_3^-]$, and a pronounced increase of $[\text{CO}_2]$ and $[\text{H}^+]$. Changing carbonate chemistry conditions are likely to modulate key physiological processes in coccolithophores (Holtz et al., 2015; Muller and Nisbet, 2014; Rokitta et al., 2012) thereby

^{*} Corresponding author at: Düsternbrooker Weg 20, 24105 Kiel, Germany. Tel.: +49 4316004258.

E-mail addresses: lbach@geomar.de (L.T. Bach), uriebesell@geomar.de (U. Riebesell), mgutowska@mbari.org (M.A. Gutowska), luisa.federwisch@awi.de (L. Federwisch), kai.schulz@scu.edu.au (K.G. Schulz).

¹ Present address: Division of Molecular Microbial Ecology, Monterey Bay Aquarium Research Institute, Moss Landing, CA 95039, USA.

² Present address: Division of Benthic–pelagic Processes, Alfred Wegener Institute Helmholtz Centre for Polar and Marine Research, 27568 Bremerhaven, Germany.

³ Present address: Centre for Coastal Biogeochemistry, School of Environmental Science and Management, Southern Cross University, 2480 Lismore, Australia.

affecting their calcification rates (Riebesell et al., 2000). However, there is presently controversy whether ocean acidification will promote or reduce calcification rates (Beaufort et al., 2011; Iglesias-Rodriguez et al., 2008a,b; Riebesell et al., 2008, 2000; Smith et al., 2012). Part of this controversy results from the absence of a conceptual understanding of the cellular and ecological mechanisms that drive observed responses in laboratory experiments and field observations.

Here, we aim to resolve the apparent discrepancies by deriving a novel physiological concept on the response of coccolithophorid calcification rates to changing carbonate chemistry conditions. We assess the validity of our concept by formulating a uniform model equation which is tested against experimental data from culture experiments on four key species (*Emiliana huxleyi*, *Gephyrocapsa oceanica*, *Calcidiscus leptoporus*, *Coccolithus pelagicus*). Furthermore, we embed this physiological concept in ecological theory – an essential second step when investigating the success of coccolithophores in the future ocean. We then compare our findings to field observations and try to assess whether near and far future carbonate chemistry conditions could impede or facilitate coccolithophorid calcification rates.

Materials and methods

Theoretical background of the concept

Metabolic rates are determined by the influence of several different physical and chemical factors. Increasing temperature, for example, accelerates metabolic rates until an optimum is reached. Further increase beyond the optimum is detrimental and leads to reduced rates until the thermal tolerance of an organism is exceeded and metabolism shuts down. The thermal window of each metabolic process will therefore always resemble an optimum curve (reviewed in Pörtner and Farrell, 2008). The same response pattern also appears when metabolic processes react to changing carbonate chemistry conditions (Bach et al., 2011). However, while the thermal reaction norm is determined by only a single physical entity (i.e. temperature), the carbonate chemistry response is composed by the interactive influence of CO_2 , HCO_3^- , CO_3^{2-} , and H^+ concentrations. Therefore, it is necessary to separate their individual impacts in order to determine which of the four components stimulate metabolic rates and which inhibit them. This is particularly relevant for calcification rates in coccolithophores which are known to be highly sensitive to changing carbonate chemistry.

Calcification-stimulating components of the carbonate system are those which are used as inorganic carbon source for intracellular CaCO_3 precipitation. Increasing availability of the inorganic carbon substrate accelerates calcification until a maximum rate is reached. However, autotrophic organisms like coccolithophores can only reach this maximum rate if carbonate chemistry conditions do not limit photosynthetic carbon fixation because calcification additionally requires large amounts of organic molecules to construct coccoliths (Brownlee and Taylor, 2004). CO_2 limitation of photosynthesis can therefore indirectly constrain calcification rates as it can lead to limited supply of essential organic compounds. It follows that calcification rates are also indirectly controlled by the influence of carbonate chemistry on photosynthetic carbon fixation. Inhibition of calcification rates occurs when rates stay sub-optimal although all metabolic processes are fully saturated with inorganic carbon substrate. This was observed in high CO_2 treatments of ocean acidification studies where rates decreased despite increasing inorganic carbon availability (Bach et al., 2011; Feng et al., 2008; Gao et al., 2009; Hoppe et al., 2011; Langer et al., 2009, 2006; Müller et al., 2010; Riebesell et al., 2000; Sciandra et al., 2003; Sett et al., 2014).

The interaction of (i) the calcification-stimulating effect of an inorganic carbon substrate used for CaCO_3 precipitation, (ii) the necessity to satisfy a minimum inorganic carbon requirement for photosynthesis so that calcification is not indirectly limited, and (iii) the negative effect of an inhibitor can be connected in a conceptual equation of the form:

$$\text{Calcification rate} = S \times [\text{substrate}] - R \times [\text{minimum requirement}] - I \times [\text{inhibitor}] \quad (1)$$

where S , R , and I are parameterizations that describe the affinity or sensitivity of per cell calcification rates to changes in $[\text{substrate}]$, $[\text{minimum requirement}]$, and $[\text{inhibitor}]$, respectively (see below). This equation constitutes the basis of the “substrate–inhibitor concept” proposed in this study.

Emiliana huxleyi is currently the best studied coccolithophore with respect to its response to changing carbonate chemistry conditions. Therefore, it is sensible to first use *E. huxleyi* data to derive a model equation which is based on the substrate–inhibitor concept and then apply this equation to other species in a second step.

The bulk of experimental studies identified HCO_3^- as the primary inorganic carbon source for calcification (Bach et al., 2013; Buitenhuis et al., 1999; Nimer and Merrett, 1993; Paasche, 1964; Rickaby et al., 2010; Sekino and Shiraiwa, 1994). It follows that calcification rate increases with increasing $[\text{HCO}_3^-]$ in the absence of an inhibitor until being saturated (Bach et al., 2013; Buitenhuis et al., 1999). Thus, the first term in Eq. (1) which represents the direct HCO_3^- dependency of calcification rate can be described by a hyperbolic function by analogy to a Michaelis–Menten kinetic:

$$S[\text{substrate}] = \frac{a[\text{HCO}_3^-]}{b + [\text{HCO}_3^-]} \quad (2)$$

where a and b parameterize the stimulation of calcification rates by increasing $[\text{HCO}_3^-]$ (units given in Table 1).

CO_2 is an important substrate for photosynthesis and cell growth (Bach et al., 2013, 2011; Paasche, 1964; Rost et al., 2003; Schulz et al., 2007). Relatively low CO_2 concentrations (e.g. below $\sim 7 \mu\text{mol kg}^{-1}$ in *E. huxleyi*) have been shown to induce a sharp reduction of cellular growth and therefore indirectly also of calcification rates (Bach et al., 2013, 2011; Sett et al., 2014). The reason for this sharp reduction was identified to be diffusive CO_2 loss which increased exponentially at the same CO_2 threshold as the exponential decline of growth and calcification rates occurred (Rost et al., 2006, 2003) and cannot be fully compensated by active inorganic carbon uptake (Bach et al., 2013; Hopkinson et al., 2011). Accordingly, leakage of CO_2 out of the cells led to pronounced inorganic carbon limitation of photosynthesis (Bach et al., 2013; Rost et al., 2006, 2003) and hence, exerts a strong indirect control on calcification rates. However, the influence of CO_2 concentration is negligible when its minimum level needed to saturate growth is exceeded (Bach et al., 2011; Sett et al., 2014). The indirect influence of sub-saturating CO_2 on calcification rates is described as:

$$R[\text{minimum requirement}] = e^{-c[\text{CO}_2]} \quad (3)$$

where the constant c determines when the indirect CO_2 limitation comes into play (units given in Table 1). The power law function used here has the advantage that it is able to reproduce the pattern observed in CO_2 leakage (see above) as it exerts a strong influence of $[\text{CO}_2]$ when its concentration is low but becomes negligible when it exceeds a certain threshold.

Inhibition of calcification rate has been identified to be induced by protons (Bach et al., 2011). High seawater H^+ concentrations can reduce the electrochemical gradient between the cytosol and seawater thereby potentially impairing the efflux of protons, a byproduct of CaCO_3 precipitation from Ca^{2+} and HCO_3^- , out of the cells (Suffrian et al., 2011; Taylor et al., 2012, 2011). Inhibition of

Table 1

Maximum measured calcite to organic carbon (PIC:POC) ratio and maximum population mean coccosphere diameter of the four coccolithophore investigated here. (Values were extracted from data by Bach et al., 2013, 2012, 2011; Langer et al., 2006; Sett et al., 2014, and this study). Maximum values for PIC:POC and coccosphere diameter are a good indicator for the species' calcification and cell size potential. Note, however, that each species can have lower PIC:POC ratios and be smaller under non-optimal carbonate chemistry conditions. Sensitivity parameters (a , b , c , d) of calcification rates were obtained by fitting measured calcification rates of 4 coccolithophore species (given in table S1) with Eq. (5). Note that their units need to be a = dimensionless, b = mol kg⁻¹, c and d = kg mol⁻¹ and concentrations of CO₂, HCO₃⁻ and H⁺ in mol kg⁻¹ in order to get a dimensionless factor for calcification rates from Eq. (5). Carbonate chemistry conditions where calcification rates either reach 50% of their maxima (OPT_{1/2} – i.e. left of the optimum; Fig. 3) or decrease down to 50% after having reached maximum values (SubOPT_{1/2} – i.e. right of the optimum; Fig. 3) were calculated from pCO₂ and TA determined in Fig. 3. R² values determine to what extent a fit with Eq. (5) is able to reproduce the data. For further analysis of the fit quality see Fig. 1.

	<i>E. huxleyi</i>	<i>G. oceanica</i>	<i>C. leptoporos</i>	<i>C. pelagicus</i>
Max. PIC:POC (mol:mol)	1.2	2.4	2.2	2.6
Max. coccosphere diameter (μm)	4.8	6.1	14.7	15.3
a (dimensionless)	9.56E-01	1.06E+00	2.31E+05	2.55E+00
b (mol kg ⁻¹)	7.04E-04	1.16E-04	3.55E+02	2.42E-03
c (kg mol ⁻¹)	2.10E+06	5.26E+05	2.19E+05	3.01E+05
d (kg mol ⁻¹)	8.27E+06	2.64E+07	3.76E+07	3.18E+07
OPT _{1/2} (CO ₂ , HCO ₃ ⁻ , H ⁺ in μmol kg ⁻¹)	0.8, 829, 0.0009	1.4, 1023, 0.0013	4.4, 1478, 0.0028	3.1, 1338, 0.0022
subOPT _{1/2} (CO ₂ , HCO ₃ ⁻ , H ⁺ in μmol kg ⁻¹)	111, 2269, 0.0458	46, 2173, 0.02	66, 2220, 0.0278	57, 2202, 0.0242
R ²	0.82	0.81	0.93	0.84

calcification rates is assumed to be linearly correlated with increasing H⁺ concentrations. This assumption is based on experimental results where a linear decrease of calcification rates was observed when cells were cultured under calcification-saturated inorganic carbon availability but exposed to increasing [H⁺] (Bach et al., 2011; Sett et al., 2014; this study). Thus, sensitivity to the inhibitor is defined as:

$$I[\text{inhibitor}] = d[\text{H}^+] \quad (4)$$

where the constant d parameterizes the sensitivity to protons (units given in Table 1).

Connecting Eqs. 2–4 according to the concept shown in Eq. (1) yields:

$$\text{Calcification rate} = \frac{a[\text{HCO}_3^-]}{b + [\text{HCO}_3^-]} - e^{-c[\text{CO}_2]} - d[\text{H}^+] \quad (5)$$

Since calcification rate depends on three different variables in this equation (HCO₃⁻, CO₂, H⁺), there are inevitably an infinite number of possible combinations for the fit parameters a , b , c , and d . This has two major implications for the use of this equation in an optimization procedure. First, a , b , c , and d must be constrained within useful ranges before starting the optimization procedure (see Section 'Fit procedure with experimental data' for further details). Second, a , b , c , and d have no physiological meaning and can therefore only be used for calculations of calcification rates after the optimization procedure but not for further biological interpretations.

Fit procedure with experimental data

Measured but normalized (see below) calcification rates of *E. huxleyi* (Bach et al., 2013, 2012, 2011), *G. oceanica* (Sett et al., 2014), *C. leptoporos* (Langer et al., 2006), *C. pelagicus* (this study; Table 3) were fitted in a non-linear least squares fit procedure with Eq. (5) to corresponding HCO₃⁻, CO₂, and H⁺ (free scale) concentrations using the function *lsqnonlin* in MATLAB (the Mathworks). The

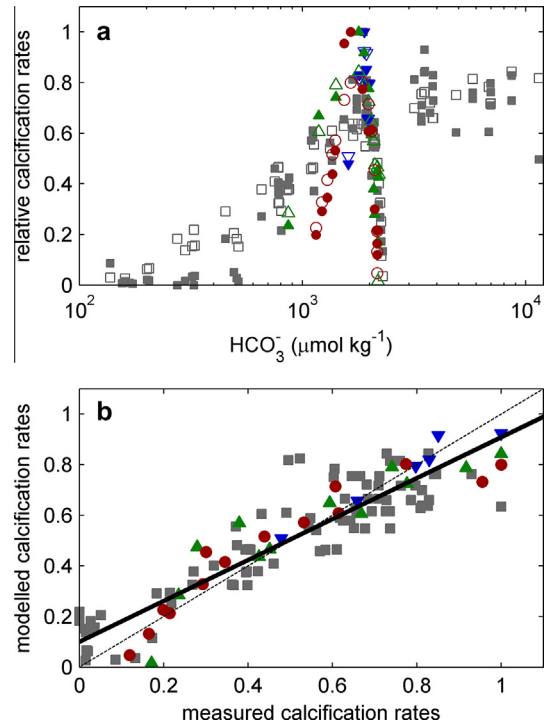


Fig. 1. (a) Comparison between measured calcification rates (normalized to the measured maximum rate determined for each species; Table S1) and modelled calcification rates on a HCO₃⁻ gradient. Modelled calcification rates were calculated using Eq. (5) and fit parameters given in Table 1 with the same carbonate chemistry data as determined for the measured values. Empty and full symbols denote modelled and measured calcification rates, respectively. Gray squares = *E. huxleyi*, blue triangles = *C. leptoporos*, green pyramids = *G. oceanica*, red dots = *C. pelagicus*. (b) Modelled vs. measured calcification rates (normalized to the maximum rate determined for each species, Table S1). The thin dotted black line denotes the 1:1 ratio and therefore the space where modelled and measured calcification rates would perfectly match. The thick black line is the linear regression ($y = 0.8086x + 0.0998$, $R^2 = 0.84$). The slope of the regression is slightly below one which indicates that the model tends to overestimate calcification rates when they are very low and underestimate them when they are extremely high (see Section 'Testing and applying the model' for further details). Species color and symbol code is the same as in (a).

difficulty in this operation lies in the multitude of variables calcification rates are fitted to. While, they are usually fitted and predicted by a single carbonate chemistry parameter (e.g. pCO₂), we define in the present study that they depend on three (HCO₃⁻, CO₂, H⁺). Thus, the same fit can be achieved with a multitude of possible combinations for the coefficients a , b , c , and d which requires constraining them within reasonable ranges before the optimization procedure with the software started. After the first run with the software we tested whether we can improve the fit by changing the constrained ranges for a , b , c , and d and subsequently running the software again. The optimization was considered to be complete when further iterations of this procedure did not further improve the coefficient of determination (R²) of the fit.

Prior to fitting, all measured calcification rates were normalized to the species-specific maximal measured calcification rate so that values used in the fit procedure ranged between 0 and 1. The normalization has two major advantages. First, per cell calcification rates which vary orders of magnitude among species (e.g. ~10 pg cell⁻¹ d⁻¹ in *E. huxleyi* vs. ~300 pg cell⁻¹ d⁻¹, in *C. pelagicus*) can be compared in one plot. Second, calculated calcification rates obtained after a fit with the normalized data represent a carbonate-chemistry dependent factor which facilitates application in other models. Nevertheless, in case real per cell calcification rates are required they can be back calculated by multiplying

relative calcification rates from the fit with Eq. (5) with the species-specific maximum measured rate. Both, absolute and normalized calcification rates are given in Table S1.

For Fig. 3, we created a $p\text{CO}_2$ gradient ranging from 0 to 2000 μatm at a constant TA of 2350 $\mu\text{mol kg}^{-1}$ and calculated $[\text{CO}_2]$, $[\text{HCO}_3^-]$ and $[\text{H}^+]$ for this gradient as described by Zeebe and Wolf-Gladrow (2001) using equilibrium constants determined by Roy et al. (1993) ($S = 35$, $T = 15^\circ\text{C}$, $P = 0$ dbar, no nutrients). Species specific calcification rates for each $p\text{CO}_2$ level of the created gradient was subsequently calculated with corresponding $[\text{CO}_2]$, $[\text{HCO}_3^-]$ and $[\text{H}^+]$ and known sensitivity parameters a , b , c , and d (obtained from the fit procedure with measured calcification rates; see above) using Eq. (5). This procedure was also adopted for Figs. 2a and 8 with the difference that we did not create a $p\text{CO}_2$ gradient for these figures but instead a whole matrix of carbonate chemistry conditions. $[\text{CO}_2]$, $[\text{HCO}_3^-]$ and $[\text{H}^+]$ calculated for each grid point in the matrix and the sensitivity parameters a , b , c , and d for *E. huxleyi* (Table 1) were used to create the contour plots.

Substrate–inhibitor interaction test with *E. huxleyi*

The substrate–inhibitor interaction (Fig. 2b) was tested with *E. huxleyi* (strain B92/11) in sterile-filtered (0.2 μm) nutrient-replete ($\text{NO}_3^- = 64 \mu\text{mol kg}^{-1}$; $\text{PO}_4^{3-} = 4 \mu\text{mol kg}^{-1}$; $\text{SeO}_2 = 10 \text{ nmol kg}^{-1}$;

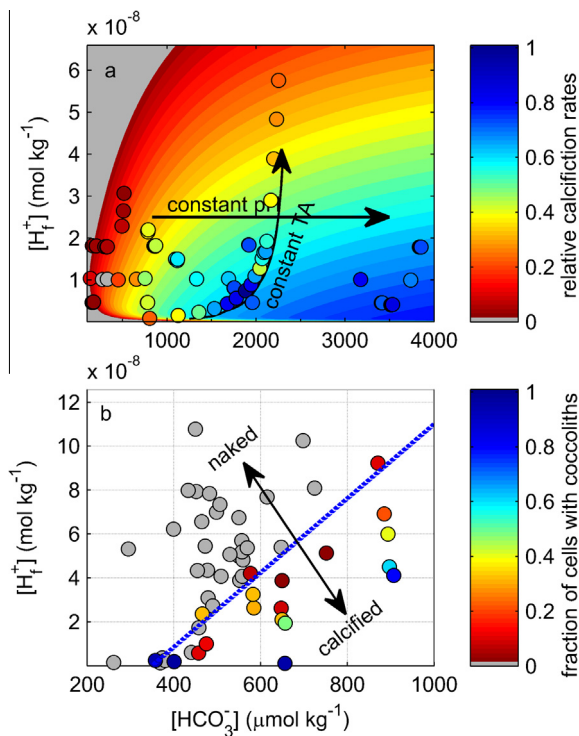


Fig. 2. Response of *E. huxleyi* to individual carbonate system parameters. (a) Relative calcification rates shown in a $[\text{H}^+]$ and $[\text{HCO}_3^-]$ grid. Contour-lines were calculated from carbonate chemistry conditions (CO_2 , HCO_3^- , H^+) with Eq. (5) using sensitivity coefficients (a , b , c , d) obtained from a fit of the *E. huxleyi* dataset. Data points represent underlying calcification rates (*E. huxleyi*; B92/11) that have been used for the fit ($R^2 = 0.82$; see Section ‘Testing and applying the model’ for details, data taken from Bach et al., 2013, 2011, 2012). The colors indicate relative calcification rates with 1 being the measured maximum (Table S1). (b) Carbonate chemistry conditions at which *E. huxleyi* was calcifying (colored) or was not calcifying (gray). The colors indicate the fraction of 200 investigated cells within a culture that were calcifying (with 1 = dark blue being 100%) after 9 h of incubation in light conditions (Table 2). Note that a larger fraction of cells starting calcification within the incubation period indicates more favorable HCO_3^- and H^+ concentrations. The dashed blue line (arbitrary) separates calcifying from non-calcifying conditions. (For interpretation of the references to color in this figure legend, the reader is referred to the web version of this article.)

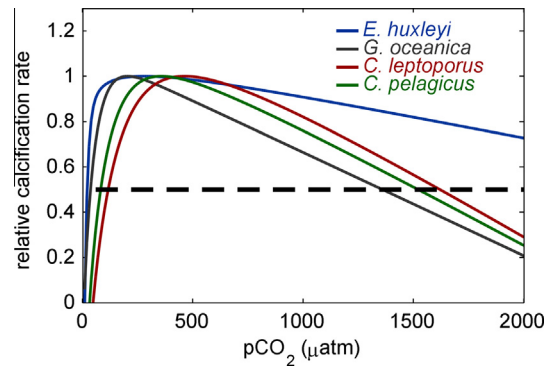


Fig. 3. Calcification rates of four different coccolithophore species in response to increasing $p\text{CO}_2$ at constant total alkalinity. Species-specific calcification rates were calculated with Eq. (5) using fit parameters given in Table 1. Calculated rates were normalized to the calculated maximum rate of each species in order to facilitate comparison of the four species within the same graph. The $p\text{CO}_2$ levels where optimum curves cross the dashed line denote the ‘50% maximum calcification rate carbonate chemistry conditions’ (i.e. $\text{OPT}_{1/2}$ on the left of the optimum and $\text{subOPT}_{1/2}$ on the right of the optimum; Table 1).

f/4 concentrations of a trace metal and vitamin mixture (Guillard and Rytner, 1962); 2 mL kg^{-1} of natural North Sea water) artificial seawater ($S = 35$; prepared as described in Kester et al. (1967) but without initial additions of NaHCO_3) at 15°C and a light intensity of $150 \mu\text{mol m}^{-2} \text{s}^{-1}$ in a 16:8 light:dark cycle. Dissolved inorganic carbon (DIC) and total alkalinity (TA) of the culture medium were adjusted by additions of NaHCO_3 , HCl , and NaOH . Cells were acclimated in autoclaved 500 mL polycarbonate bottles (Nalgene) to calcification-inhibiting carbonate chemistry conditions (TA and DIC = $500 \mu\text{mol kg}^{-1}$) prior to the main experiment for at least 10 generations. Aliquots from this pre-culture were incubated ($140\text{--}300 \text{ cells mL}^{-1}$) in autoclaved 2L polycarbonate bottles for 4–5 generations (yielding $\sim 5000 \text{ cells mL}^{-1}$) in 14 potentially calcification-inhibiting carbonate chemistry conditions with differing TA and DIC. Cell cultures were then inspected for coccoliths in an inverse light microscope using two orthogonally aligned polarized filters. In case coccoliths could not be detected, the non-calcifying culture was split into four sub-volumes (310 mL, Schott Duran) and manipulated with different amounts of NaHCO_3 , HCl , or NaOH to yield new carbonate chemistry conditions. After the sub-volumes were incubated for 9 h in light conditions, 200 cells were once more carefully inspected for coccoliths using cross-polarized light- and scanning electron microscopy in case results from light microscopy needed to be backed up.

Samples for DIC and TA were taken before splitting cell cultures and at the end of the experiments. Both, TA and DIC samples were filtered (0.7 and 0.2 μm , respectively) and stored (DIC in gas tight bottles without headspace) at 4°C until measurements. DIC was measured by an infra-red absorption method using an AIRICA system (MARIANDA), equipped with a LICOR LI-7000, while TA was measured in an open cell titration using a Metrohm 794 Basic titrino as described in Dickson et al. (2007). Remaining carbonate chemistry parameters were calculated with CO2SYS (Lewis and Wallace, 1998) using equilibrium constants determined by Roy et al. (1993). All measured or calculated data of this substrate–inhibitor compensation experiment is reported in Table 2.

Culture experiments with *Coccolithus pelagicus* ssp. braarudii

The response of growth, particulate organic carbon (POC) production, and calcification rates of *Coccolithus pelagicus* ssp. braarudii (strain PLY182G) to increasing $[\text{CO}_2]$ at constant TA ($2328 \pm 9 \mu\text{mol kg}^{-1}$) was tested as described in (Bach et al., 2012, 2011). Briefly: Cells were grown under controlled conditions

Table 2

Carbonate chemistry and calcification data of the substrate–inhibitor interaction experiment with *E. huxleyi* (Fig. 2b). The percentage of 200 cells possessing/producing coccoliths was investigated by means of cross-polarized light microscopy which allows detection of internal coccoliths. These birefringence measurements were backed up with scanning electron microscopy (SEM) investigations when the presence of coccoliths could not be unequivocally determined. In case of discrepancies among the two methods, we relied on SEM investigations since this is the most reliable approach. Percentages marked in 'bold' are those where coccoliths were found.

TA ($\mu\text{mol kg}^{-1}$)	DIC ($\mu\text{mol kg}^{-1}$)	pH free scale	H ⁺ (nmol kg^{-1})	fCO ₂ (μatm)	HCO ₃ ⁻ ($\mu\text{mol kg}^{-1}$)	CO ₃ ²⁻ ($\mu\text{mol kg}^{-1}$)	CO ₂ ($\mu\text{mol kg}^{-1}$)	Ω_{calcite}	Cells with coccoliths (%)	Coccoliths found by means of SEM
469.5	488.7	7.13	74.9	957	449	4	35.8	0.10	0.4	No
485.6	494.5	7.23	59.3	777	460	5	29.1	0.12	0	
497.6	494.9	7.34	45.5	602	465	7	22.6	0.16	0.5	No
509.4	490.4	7.50	31.5	417	465	10	15.6	0.23	0	No
522.9	490.4	7.62	23.8	315	466	13	11.8	0.31	0	No
636.0	668.6	7.11	77.1	1344	613	5	50.3	0.13	0	
678.1	679.4	7.36	44.0	801	640	10	30.0	0.23	0.5	No
690.9	686.6	7.40	39.5	728	648	11	27.3	0.26	2.4	
707.1	685.4	7.54	28.9	534	650	15	20.0	0.36	9.3	
723.1	688.6	7.63	23.2	432	654	19	16.2	0.45	32.9	
572.9	585.4	7.23	58.4	905	545	6	33.9	0.15	0	
580.2	592.8	7.24	58.1	913	552	6	34.2	0.15	0	
583.1	589.5	7.29	51.5	809	552	7	30.3	0.17	0	
590.9	589.2	7.36	43.7	689	555	8	25.8	0.20	0	
594.8	589.8	7.39	40.8	646	556	9	24.2	0.22	0	Yes
877.8	538.8	8.71	2.0	22	401	137	0.8	3.26	97.6	Yes
463.6	491.7	7.05	89.5	1135	446	3	42.5	0.08	0	
501.1	498.4	7.34	45.5	606	469	7	22.7	0.16	0	
539.5	501.3	7.67	21.3	289	476	15	10.8	0.36	0	No
600.2	509.8	8.00	10.0	135	473	32	5.0	0.75	12.6	
658.1	506.2	8.25	5.6	72	450	54	2.7	1.28	9.6	
586.1	595.3	7.27	54.3	859	556	7	32.2	0.16	0	
597.4	598.9	7.33	46.4	743	563	8	27.8	0.19	0.5	No
612.6	604.1	7.42	37.8	614	571	10	23.0	0.24	7.8	
628.4	604.0	7.56	27.7	452	573	14	16.9	0.33	31.8	
640.5	606.1	7.64	23.1	378	575	17	14.2	0.40	30.7	
724.9	462.5	8.58	2.6	28	368	93	1.0	2.22	93.7	
521.8	488.3	7.63	23.3	307	464	13	11.5	0.32	31.9	Yes
892.1	951.7	7.07	84.6	2085	867	7	78.1	0.16	11	
913.5	951.2	7.19	64.8	1625	881	9	60.9	0.22	21.2	
926.2	959.4	7.22	60.8	1542	892	10	57.8	0.23	39.6	
939.8	949.5	7.35	44.2	1124	894	14	42.1	0.32	61.4	
954.1	946.0	7.47	34.2	871	896	18	32.6	0.42	79.7	
317.0	326.8	7.11	77.4	659	300	3	24.7	0.06	0	
737.9	380.2	8.84	1.4	11	260	120	0.4	2.86	0	
650.5	442.7	8.45	3.6	38	372	70	1.4	1.66	0	
977.8	550.2	8.87	1.4	14	368	182	0.5	4.34	0	No
1663.5	1028.5	8.93	1.2	22	655	373	0.8	8.89	95.4	
421.0	428.7	7.21	62.3	705	398	4	26.4	0.10	0	
519.2	538.2	7.16	70.0	988	496	5	37.0	0.11	0	
543.9	537.5	7.39	40.8	588	507	8	22.0	0.20	0	
590.2	582.6	7.41	38.9	608	550	9	22.8	0.23	0	
737.2	691.4	7.71	19.4	362	655	23	13.6	0.54	48.5	
450.8	471.9	7.10	79.9	981	432	4	36.7	0.09	0	
485.8	480.5	7.36	43.3	558	453	7	20.9	0.17	0	
531.9	482.2	7.76	17.4	225	456	18	8.4	0.42	0	
628.6	489.3	8.21	6.1	76	439	48	2.9	1.14	1	Yes
772.0	485.9	8.62	2.4	26	379	106	1.0	2.53	1	Yes
526.3	548.3	7.13	73.4	1053	504	5	39.5	0.11	0	
558.3	562.9	7.29	50.7	761	527	7	28.5	0.17	0	
715.1	776.6	6.99	102.6	2031	696	5	76.1	0.11	0	
746.4	790.8	7.09	80.9	1662	723	6	62.3	0.14	0.5	No
785.9	800.4	7.29	51.3	1094	750	10	41.0	0.23	2	Yes
208.9	233.1	6.81	154.1	874	200	1	32.8	0.02	0	

(RUBARTH climate chamber) in sterile-filtered nutrient replete artificial seawater (see above) at 15 °C and a light intensity of 170 $\mu\text{mol m}^{-2} \text{s}^{-1}$ in a 16:8 light:dark cycle. Cells were acclimated to experimental conditions for 10 generations in autoclaved 500 mL glass bottles (Schott Duran) and subsequently transferred with relatively low initial cell numbers (<40 cells mL^{-1}) into 17 autoclaved glass bottles containing seawater with the same chemical conditions. Cell numbers at the beginning and the end of the experiments were measured with an Accuri C6 flow cytometer (BD Biosciences). Carbonate chemistry conditions were adjusted by adding calculated amounts of Na_2CO_3 and HCl to the seawater medium. DIC and TA was sampled and measured before transferring the acclimated cells and at the end of the experiments as described

above. Three TA measurements from the end of the experiments failed and had to be approximated from initial TA and the build-up of particulate inorganic carbon (PIC) as:

$$TA_{\text{end}} = TA_{\text{initial}} - 2(\text{PIC}_{\text{build-up}}) \quad (6)$$

where $\text{PIC}_{\text{build-up}}$ is given in $\mu\text{mol kg}^{-1}$. $[\text{CO}_2]$, $[\text{HCO}_3^-]$ and $[\text{H}^+]$ were calculated for each treatment from the mean of initial and final DIC and TA measurements with CO2SYS as described above.

Sampling started 2 h after the onset of the light period and lasted no longer than 2 h. Total particulate carbon (TPC) and particulate organic carbon (POC) samples were filtered onto GF/F filters (combusted at 500 °C for 12 h) and stored in combusted (500 °C, 12 h) glass petri dishes at -20 °C. Prior to analysis, POC samples

were transferred into a desiccator and placed for 4 h above fuming (37%) HCl that removed all inorganic carbon. POC samples were dried overnight after the acid treatment at 60 °C. TPC samples were dried for the same time and temperature without the previous acid treatment in a separate oven. The amount of TPC and POC on filters was analyzed with a C/N analyzer (Hekatech). Particulate inorganic carbon (PIC) was calculated by subtracting POC from TPC.

Growth rates μ (d^{-1}) were calculated from initial and final measured cell densities (N_{t_0} , $N_{t_{fin}}$) as:

$$\mu = \frac{\ln(N_{t_{fin}}) - \ln(N_{t_0})}{d} \quad (7)$$

where the growth period (d) is given in days.

POC production and calcification rates were calculated as the product of POC $cell^{-1}$ or PIC $cell^{-1}$ and μ , respectively. All measured or calculated data of this experiment with *C. pelagicus* is reported in Table 3.

Results and discussion

Testing and applying the model

Measured calcification rates of *E. huxleyi*, *G. oceanica*, *C. leptopus*, and *C. pelagicus* (Bach et al., 2013, 2011; Langer et al., 2006; Sett et al., 2014; this study) grown in a large variety of carbonate chemistry, but otherwise identical, culture conditions (an important aspect covered in Section ‘The influence of culture conditions’) were fitted against CO_2 , HCO_3^- and H^+ with Eq. (5). The fits yielded coefficients of determination (R^2) ranging between 0.81 and 0.93 (Table 1). Visually comparing measured with modelled calcification rates plotted on a HCO_3^- gradient shows that the substrate–inhibitor principle implemented in Eq. (5) can retrace the most important patterns observed in the data (Fig. 1a). Accordingly, measured and modelled calcification rates correlate reasonably well ($R^2 = 0.84$, Fig. 1b). Largest discrepancies between data and model fit occur at rather extreme calcification rates. Here the model tends to slightly overestimate calcification rates when they are very low and slightly underestimates them when they are peaking (Fig. 1b). The reason for this is that Eq. (5) has under certain circumstances problems to reproduce abrupt changes in calcification rates when they occur on a very narrow range of carbonate chemistry conditions. The problem could be solved by adding extra terms to Eq. (5), thereby increasing its complexity. In this study, however, we chose not to sacrifice the simplicity of the model on the expense of rather marginal improvements in the fit quality in order to keep the discussion focused on the substrate–inhibitor concept.

The fit parameters a , b , c , and d (Table 1) of the four coccolithophore species can be used with Eq. (5) to calculate the species’ relative calcification rates as a function of $[H^+]$, $[HCO_3^-]$, and $[CO_2]$. This is shown with the example of *E. huxleyi* in Fig. 2a where calculated calcification rates are compared with measured values in a matrix of carbonate chemistry conditions. Blue areas in this figure represent calcification-favorable carbonate chemistry environments with high substrate (HCO_3^-) availability, low inhibitor (H^+) concentrations, and sufficient CO_2 supply for photosynthesis so that calcification is not hindered indirectly (note that low CO_2 conditions occur at low HCO_3^- and H^+ in Fig. 2a). These results have several interesting implications which shall be discussed in more detail in the following.

Ocean acidification (increasing CO_2 at constant total alkalinity) is represented in Fig. 2a by a curved line which starts at relatively low $[CO_2]$ and $[H^+]$ where calcification is indirectly limited by the insufficient CO_2 supply for photosynthesis. At intermediate CO_2 , calcification rates reach their optimum (and cross the blue area

Table 3 Carbonate chemistry and physiological growth data of experiments with *C. pelagicus*. Mean TA and DIC were calculated as average of initial and final values. pH, pCO_2 , HCO_3^- , CO_3^{2-} , and CO_2 were calculated from mean TA and DIC as described in Section ‘Substrate–inhibitor interaction test with *E. huxleyi*’. POC = particulate organic carbon, TPC = total particulate carbon, PIC = particulate inorganic carbon.

Measured t_0				Calculated mean				Physiological data										
TA t_0 ($\mu mol\ kg^{-1}$)	DIC t_0 ($\mu mol\ kg^{-1}$)	TA t_{fin} ($\mu mol\ kg^{-1}$)	DIC t_{fin} ($\mu mol\ kg^{-1}$)	Mean TA ($\mu mol\ kg^{-1}$)	Mean DIC ($\mu mol\ kg^{-1}$)	pH (free scale)	fCO_2 (μatm)	HCO_3^- ($\mu mol\ kg^{-1}$)	CO_3^{2-} ($\mu mol\ kg^{-1}$)	CO_2 ($\mu mol\ kg^{-1}$)	Growth rate μ (d^{-1})	POC quota ($\mu g\ cell^{-1}$)	POC production ($\mu g\ cell^{-1}\ day^{-1}$)	TPC quota ($\mu g\ cell^{-1}$)	TPC production ($\mu g\ cell^{-1}\ day^{-1}$)	PIC quota ($\mu g\ cell^{-1}$)	PIC production ($\mu g\ cell^{-1}\ day^{-1}$)	PIC:POC (mol:mol)
2340.0	1656.4	2245.5*	1568.8	2292.8	1612.6	8.78	55	1150	461	2.0	0.33	182	60	355	117	173	57	1.0
2330.7	1694.6	2178.2	1583.5	2254.4	1639.0	8.71	68	1221	415	2.6	0.42	159	67	359	151	201	84	1.3
2336.7	1735.5	2167.4	1623.3	2250.6	1678.9	8.65	82	1289	386	3.1	0.45	151	68	372	167	221	100	1.5
2326.2	1768.1	2125.4	1611.0	2225.8	1689.6	8.61	92	1324	362	3.5	0.46	147	68	447	206	266	126	1.8
2325.5	1789.6	2101.8	1621.2	2213.6	1705.4	8.58	103	1359	343	3.8	0.49	139	68	397	195	258	126	2.0
2325.8	1812.1	2071.5*	1636.3	2198.6	1724.2	8.53	117	1400	320	4.4	0.48	160	77	479	230	319	153	2.4
2336.1	1914.8	1949.7	1657.5	2142.9	1786.1	8.37	187	1538	241	7.0	0.39	194	115	661	390	466	275	2.4
2349.7	1977.3	1963.7	1737.8	2156.7	1857.5	8.27	251	1644	204	9.4	0.59	190	112	678	400	488	288	2.6
2326.0	2118.1	2053.0*	1900.4	2189.5	2069.2	8.03	498	1859	132	18.7	0.59	189	111	567	334	378	223	2.0
2337.5	2189.2	2098.1	2007.4	2217.8	2098.3	7.87	756	1972	98	28.3	0.58	209	121	511	296	302	175	1.4
2319.1	2228.2	2152.2	2082.3	2235.7	2155.2	7.76	1013	2039	78	37.9	0.55	230	127	552	304	322	177	1.4
2320.9	2286.5	2193.3	2143.2	2257.1	2214.9	7.64	1370	2102	61	51.3	0.34	275	93	529	180	255	87	0.9
2318.4	2325.5	2234.6	2226.8	2276.5	2276.1	7.51	1903	2158	47	71.3	0.32	277	89	470	150	193	62	0.7
2321.2	2350.9	2214.8	2206.6	2268.0	2278.7	7.47	2062	2159	43	77.2	0.27	319	86	495	134	176	62	0.6
2320.5	2371.4	2209.0	2201.1	2264.7	2286.2	7.44	2230	2163	40	83.5	0.26	267	69	399	104	132	34	0.5

* Estimated with Eq. (6).

in Fig. 2a) since CO_2 demand for photosynthesis is satisfied, HCO_3^- substrate is sufficiently available, and inhibition by H^+ is still relatively low. At high CO_2 , the inhibition by H^+ becomes the dominant factor leading to decreasing calcification rates (Fig. 2a; see also Bach et al., 2013, 2011; Sett et al., 2014). In a carbonate chemistry scenario where $[\text{HCO}_3^-]$ increases at constant $[\text{H}^+]$ (straight horizontal line in Fig. 2a), calcification rates increase hyperbolically. A steep increase from low to intermediate substrate availability is followed by saturation toward higher substrate concentrations.

A particularly interesting implication of the modelled results is that the inhibition of calcification rates by H^+ could potentially be compensated by increased HCO_3^- substrate availability. For example, at $2 \text{ nmol kg}^{-1} [\text{H}^+]$, calcification rates can be similarly high as at $1 \text{ nmol kg}^{-1} [\text{H}^+]$ provided that $[\text{HCO}_3^-]$ is also approximately twice as high (Fig. 2a). Possibly, elevated HCO_3^- availability and therefore increased supply of inorganic carbon to the coccolith vesicle, enables the cells to compensate to a certain degree the reduction of $[\text{CO}_3^{2-}]$ at the site of calcification which is caused by increased intra-cellular $[\text{H}^+]$. In order to test this substrate–inhibitor compensation, we cultured *E. huxleyi* for 10 generations at dissolved inorganic carbon (DIC) concentrations and total alkalinity (TA) below $500 \mu\text{mol kg}^{-1}$ which suppresses calcification (Bach et al., 2013). These cell cultures were then enriched with different amounts of NaHCO_3 , NaOH , or HCl and subsequently inspected by cross-polarized light- and scanning electron microscopy to check the cells' ability to form coccoliths under various combinations of $[\text{HCO}_3^-]$ and $[\text{H}^+]$ (see Section 'Results and discussion' for further detail). This test shows that the negative influence of $[\text{H}^+]$ can be compensated at least to a certain degree by elevated availability of HCO_3^- and increases the confidence in the substrate–inhibitor concept described here (Fig. 2b, Table 2).

Fig. 3 shows the calculated response of the four investigated species to increasing seawater $p\text{CO}_2$ at constant TA, the typical ocean acidification scenario. The reaction norm for this carbonate chemistry scenario was calculated with species-specific fit parameters a , b , c , and d (Table 1) and $[\text{H}^+]$, $[\text{HCO}_3^-]$, and $[\text{CO}_2]$ using Eq. (5) (see Section 'Fit procedure with experimental data' for details on the calculation). All four species show optimum curve reaction norms over the full $p\text{CO}_2$ spectrum which is in accordance with what can be expected for such a carbonate chemistry scenario (Bach et al., 2011; Langer et al., 2006; Sett et al., 2014, this study). Calcification rates of *E. huxleyi* – the smallest species – increase most steeply in the low $p\text{CO}_2$ range and are least sensitive toward the high end. The initial increase in the slightly larger species *G. oceanica* is less steep and the species reacts more sensitively toward higher $p\text{CO}_2$ (higher $[\text{H}^+]$). *C. pelagicus* and *C. leptoporus* – the two largest species investigated here – have their calcification optima shifted to considerably higher $p\text{CO}_2$ levels compared to the smaller species. Yet, their sensitivity at high $p\text{CO}_2$ is comparable to that of *G. oceanica* (Fig. 3).

Observed variability in sensitivities among these species nicely reflects their different surface to volume and calcite to organic carbon (PIC:POC) ratios. The two larger species *C. pelagicus* and *C. leptoporus* with a lower surface to volume ratio require more inorganic carbon substrate in their immediate proximity to saturate inorganic carbon flux into the cell (Flynn et al., 2012; Rickaby et al., 2010; Wolf-Gladrow and Riebesell, 1997), the presumed reason why their "50% maxima" of calcification rates ($\text{OPT}_{1/2}$, Table 1) are reached at higher $p\text{CO}_2$. Steeper decline of calcification rates after the optimum (Fig. 3) of *G. oceanica*, *C. leptoporus*, and *C. pelagicus* compared to *E. huxleyi* could be due to their significantly higher degree of calcification (maximum PIC:POC ratios are 2.2 – 2.6 in *G. oceanica*, *C. leptoporus*, and *C. pelagicus* vs. 1.2 in *E. huxleyi*; Table 1). An increased PIC:POC ratio indicates that cells have to release relatively more H^+ stemming from the intracellular calcification reaction ($\text{Ca}^{2+} + \text{HCO}_3^- \rightarrow \text{CaCO}_3 + \text{H}^+$) compared to cells with low

PIC:POC. Thus, maintaining a steady H^+ efflux could become increasingly difficult if the cells are more heavily calcified, because these cells have to discharge larger quantities of H^+ under unfavorable conditions than less calcified ones.

At first, it may be somewhat surprising that one can so easily unify the calcification responses of four different coccolithophores species to changing carbonate chemistry conditions in one simple concept although the Isochrysidales group (*G. oceanica* and *E. huxleyi*) diverged from the Coccolithales (*C. leptoporus* and *C. pelagicus*) ~250 million years ago (Liu et al., 2010). However, the fact that (1) inorganic carbon is essential for calcification and (2) that protons, when present in critical concentrations, are detrimental to every organism make this substrate–inhibitor principle rather logical. Perhaps it is so basic to the process of calcification that it applies to marine calcifiers in general.

The influence of culture conditions

Calcification rates are not exclusively determined by carbonate chemistry conditions but also by other environmental parameters such as light availability, temperature, or nutrient concentrations. All of these parameters can potentially modify the response of calcification rate to changing carbonate chemistry (De Bodt et al., 2010; Feng et al., 2008; Gao et al., 2009; Rokitta and Rost, 2012; Sciandra et al., 2003; Sett et al., 2014). In the present concept and model Eq. (5), we neglected their influence. This has two major reasons. First, a multitude of physical and chemical factors influence calcification rates and most of them have not been studied so far. Thus, it does not make sense to selectively extend the model by e.g. temperature and light intensity when other factors of equally high importance but where no data is available remain unconsidered. Second, and perhaps more importantly, we understand quite well that e.g. temperature and light intensity changes can increase or decrease calcification rates. This aspect could easily be included in our model by multiplying equation 5 with temperature and light intensity and a specific scaling factor or function. However, we understand far worse how these and/or other relevant physical and chemical factors interactively modify the cells' affinity and sensitivity to $[\text{HCO}_3^-]$, $[\text{CO}_2]$, and $[\text{H}^+]$. Affinity and sensitivity to $[\text{HCO}_3^-]$, $[\text{CO}_2]$, and $[\text{H}^+]$ are parameterized in Eq. (5) by the coefficients a , b , c , and d . In our model, a modification of a , b , c , and d by changing growth conditions (such as light or temperature conditions) would alter the shape of the reaction norm but it would not change the greater response pattern. For example, the optimum curve response pattern of calcification rates observed under increasing $p\text{CO}_2$ at constant TA (Fig. 3) would stay an optimum curve at different culture conditions. The curve progression, however, would look different. How this rearrangement of the curve progression works and which mechanisms it obeys is unfortunately poorly understood at the moment. Unraveling these mechanisms should be a key focus in future physiological studies so that we become able to reasonably integrate the interactive influence between relevant environmental factors and carbonate chemistry on coccolithophorid calcification rates in the present or any other physiological model.

In a recent study we made a first attempt on this and investigated how different temperature treatments modified the anticipated optimum curve reaction norm of calcification rate in *E. huxleyi* and *G. oceanica* to increasing $[\text{CO}_2]$ at constant TA (Sett et al., 2014). These experiments revealed: (i) The reaction norm did indeed always resemble an optimum curve in this ocean acidification mimicking carbonate chemistry manipulation, regardless of the incubation temperature. (ii) The CO_2 concentration where optimal calcification rates were reached tended to increase with temperature so that the progression of the optimum curve differed among temperature treatments. Accordingly, temperature did not

change the stimulating influence of CO_2 and HCO_3^- or the inhibiting influence of H^+ on calcification rate but it did change the organism's affinity and sensitivity to them. The potential explanation for this “optimum shift” of calcification rates toward higher CO_2 levels at higher temperatures was hypothesized to be the direct result of a temperature-accelerated metabolism which presumably profits more from the increase in inorganic carbon availability than it suffers from inhibition by higher $[\text{H}^+]$ (Sett et al., 2014).

An example where such light and/or temperature-driven affinity/sensitivity-modifications may explain seemingly inconsistent responses of calcification rates to simulated ocean acidification are the studies by Langer et al. (2009) and Hoppe et al. (2011). While Hoppe et al. reported decreasing calcification rates in a $p\text{CO}_2$ range from 200 to 1000 μatm , Langer et al. showed an optimum-curve like response over the same range (Fig. 4). Both studies followed the same experimental protocol, investigated the same *E. huxleyi* strain (RCC1256), but cultured them at different temperatures and light intensities, being 17 °C and 400 $\mu\text{mol photons m}^{-2} \text{s}^{-1}$ in Langer et al. (2009) and 15 °C and 170 $\mu\text{mol photons m}^{-2} \text{s}^{-1}$ in Hoppe et al. (2011). Higher temperature and light intensity in Langer et al. (2009) could have shifted the optimum of calcification rate toward higher $p\text{CO}_2$ because cells had a higher carbon demand due to an accelerated metabolism and an increased energy supply to cope with the inhibiting effects of elevated $[\text{H}^+]$. This optimum shift appears as different response within the ocean acidification relevant $p\text{CO}_2$ range even though the underlying physiological response is most likely the same (an optimum curve response) in both examples (Fig. 4).

“Shifting $p\text{CO}_2$ optima” may also explain variable responses observed in *E. huxleyi* strain NZEH where Iglesias-Rodriguez et al. (2008b) reported increasing calcification rates with rising $p\text{CO}_2$ while Hoppe et al. (2011) found the opposite. As in the previous example, strain NZEH can be expected to respond with the same physiological pattern in both studies. But since culture conditions were different, the optimum may be shifted to higher $p\text{CO}_2$ in Iglesias-Rodriguez et al. (2008b), thereby yielding an opposite trend in the given section of the $p\text{CO}_2$ range (Fig. 4). The presumed optimum shift in Iglesias-Rodriguez et al. (2008b) could be due to higher incubation temperature (see comparison given above), although this is not supported by the much lower absolute rates observed (Fig. 4). Alternatively, the shorter light period set up by Iglesias-Rodriguez et al. (2008b) (light:dark = 12:12 (h:h) as opposed to 16:8 in Hoppe et al. (2011), see Table 4) might have played an important role as the shorter timespan translates to a considerably lower light supply of about ~30% when integrated over the whole day. In any case, this comparison shows that experimental protocol and/or culture conditions have a profound influence on the response of coccolithophorid calcification rates to increasing $p\text{CO}_2$. In fact, all possible responses (increasing, constant, and decreasing calcification rates) have been reported for the *E. huxleyi* strain NZEH (Fig. 5). This surprisingly large method-related variability may even have the potential to obscure the variability which is incurred by genetic differences between strains. In order to test this possibility we first checked how much variability in the response to increasing CO_2 can be observed in the same strain when it was grown in a variable experimental setup (Fig. 5a and b; Table 4) and then compared this to the variability observed among strains which were grown in an identical experimental setup (Fig. 5c, Table 4). This test indicates that differences in the experimental protocol and/or culture conditions can cause at least as much variability as genetic differences between strains (Fig. 5; Table 4).

Embedding the physiological concept in ecological theory

The response of coccolithophorid calcification rates to ocean acidification has been investigated in many monoclonal culture

experiments (reviewed in Riebesell and Tortell, 2011). Results from these studies were often used to make assumptions on the role of coccolithophores in the future marine carbon cycle. Such extrapolations are questionable, however, since they are based on experiments which neither consider a potential change in coccolithophore community composition nor in absolute abundances. A change in either of these parameters has most likely a larger feedback capacity on the marine carbon cycle than a change in cellular calcification rate alone. Coccolithophore species composition can change when certain coccolithophores profit/suffer more than others from changing carbonate chemistry conditions. Their total abundance can change when the altered physiological performance under acidified conditions alters competitiveness of coccolithophores compared to other functional groups. It is therefore essential to couple physiological and ecological theory when trying to assess the role of coccolithophores in the future ocean (Kearney and Porter, 2009). In the following, a thought experiment will illustrate how this could be achieved.

Integrating a physiological into an ecological concept can be realized by application of the niche theory introduced by Hutchinson (1957). Hutchinson defined a niche as n -dimensional hypervolume where dimensions represent many different biotic and abiotic factors that control the presence of a species in a habitat. The niche can be further sub-divided into two hierarchical levels – the fundamental niche and the realized niche. The former describes the sum of abiotic conditions where an organism would live when no interference with other organisms takes place. The latter also includes interactions between organisms and thus describes the conditions where an organism actually does live (Hutchinson, 1957). In its original form the niche concept is used on a species level. We will now transform the concept from species to physiological process level and subsequently discuss if the process (in this case calcification) could be linked to the success of coccolithophores in the oceans.

The substrate–inhibitor concept (Eq. (5)) describes the fundamental niche of calcification with respect to carbonate chemistry (Fig. 3). To include the realized niche in the concept it is necessary to assume that the ability to calcify is a fitness-relevant trait. This assumption seems reasonable because if calcification was not beneficial, it would have been lost during evolution as it is associated with significant energetic costs (Brownlee and Taylor, 2004). It follows that the ability to calcify could allow them to occupy a niche that would otherwise be occupied by a competitor or would be left vacant. Conversely, a loss of calcification or a reduction of calcification rates could result in a reduced competitiveness of the coccolithophore.

The mechanism of how this could work is illustrated in Fig. 6. Here, the realized niche for calcification is constrained by a cost-benefit-threshold (CBT) above which calcification rates are high enough to pose a competitive advantage. In the complete absence of interactions between coccolithophores and competitors/grazers, the CBT is zero and the realized niche equals the fundamental niche (like in monoclonal culture experiments). As competition for resources and grazing pressure intensifies the CBT gradually increases and narrows the realized niche for calcification. If deteriorating carbonate chemistry conditions drive calcification rates below the CBT (i.e. calcification costs exceed the associated benefits) then the ability to calcify is no longer a competitive advantage. In the worst case this could lead to a replacement of coccolithophores because species which can occupy the same niche are now able to successfully compete with them.

Evolutionary adaptation may enable coccolithophores to escape replacement, either by selection on standing genetic variation or by the accumulation of beneficial *de novo* mutations (Collins et al., 2014; Jin et al., 2013; Lohbeck et al., 2012). Standing genetic variation is reflected in strain-specific responses to changing

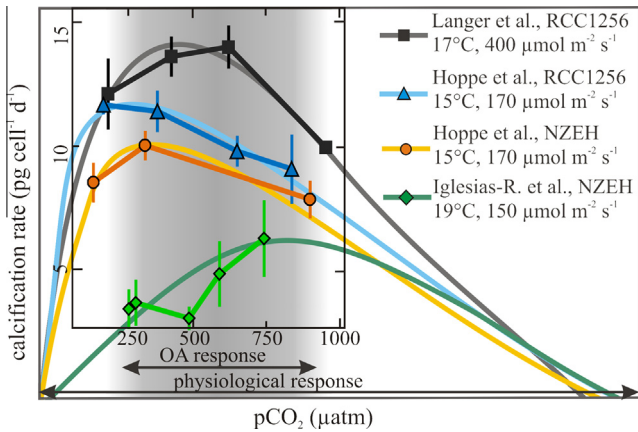


Fig. 4. Potential influence of different culture conditions on the outcome of experiments with *E. huxleyi* strains NZEH and RCC1256 (light intensities in $\mu\text{mol photons m}^{-2} \text{s}^{-1}$). This comparison is based on data reported by Langer et al. (2009), Hoppe et al. (2011), and Iglesias-Rodriguez et al. (2008b). The optimum curves (arbitrary) were added to each dataset in order to illustrate that the underlying response pattern would be similar according to the substrate–inhibitor concept, despite the large differences in the calcification response within the ocean acidification (OA) relevant range of the $p\text{CO}_2$ gradient (see Section ‘The influence of culture conditions’ for details).

carbonate chemistry (Langer et al., 2009). It increases the likelihood to find and select for genotypes within populations that are able to keep calcification rates above the CBT under continuously acidifying conditions (Fig. 4). The variability among strains in their response to changing carbonate chemistry can be substantial (Langer et al., 2009; Read et al., 2013). However, variability is difficult to quantify at the moment since there is a lack of data where genotype-specific effects can clearly be distinguished from the influence of variable culture conditions (see Section ‘The influence of culture conditions’). When this data becomes available it can be accounted for in Eq. (5) by parameterization of the constants a , b , c , and d which, in concert, determine the affinity to substrates and sensitivity to the inhibitor.

Calcification-relevant *de novo* mutations are another source of variation adaptation can act on (Collins et al., 2014). They can accumulate in populations when high calcification rates are under positive selection (Lohbeck et al., 2012). This would change affinities/sensitivities (collectively parameterized by a , b , c , and d in Eq. (5)) to HCO_3^- , CO_2 , and H^+ over time. The rate of change, however, is particularly difficult to constrain which poses a major challenge for any kind of model parameterization.

The degree by which calcification can adapt to ocean acidification is presently unknown. Cell physiological examinations found the essential H^+ efflux (stemming from the use of HCO_3^- for intracellular calcification) to become more costly with ongoing ocean acidification as the electrochemical H^+ inside-out gradient is reduced and passive proton outflow impeded (Taylor et al., 2011). Adapted cells would have to activate proton channels more frequently, adjust their membrane potential, and/or lower their internal pH (Taylor et al., 2012). Reduced intra-cellular pH would severely affect the entire cellular machinery and require other processes (e.g. photosynthesis) to co-adapt in order to keep H^+ efflux alive (Benner et al., 2013; Lohbeck et al., 2014). The obligatory H^+ efflux associated with calcification may therefore pose a fundamental constraint on adaptation which may potentially explain why ‘‘calcification crisis’’ were possible during long-lasting (thousands of years) CO_2 perturbation events (Erba and Tremolada, 2004; Erba, 2006) even though evolutionary adaptation to changing carbonate chemistry conditions is possible within one year (Jin et al., 2013; Lohbeck et al., 2012). Unraveling these fundamental constraints and the limits of adaptation should be a focus in future coccolithophore

studies because knowing them is the key information required to understand to what extent the calcification response to carbonate chemistry perturbations can be compensated by evolution.

Silicate- or cellulose-armed functional groups such as diatoms and dinoflagellates do not need to sustain the calcification-related H^+ efflux. Thus, they probably do not need to adapt in order to keep costs for the production of structural elements low. On the contrary, dinoflagellates (except for calcifying species; (Van de Waal et al., 2013)) with generally inefficient CO_2 -fixing RuBisCO enzymes (Tortell, 2000) may even profit from chemical changes since photosynthetic carbon fixation as their source of structural elements in the form of cellulose should be facilitated by the ocean acidification-associated CO_2 fertilization (Fu et al., 2008; Reinfelder, 2011). Under the assumption that any form of shell/exoskeleton protects phytoplankton against predation (as argued by Hamm and Smetacek, 2007), non-calcareous armors may be the preferable solution to realize protection in a future ocean (Fig. 7).

Implications: past, present, and future

In this section we apply the substrate–inhibitor principle in order to speculate on past, present, and future success and distribution of coccolithophores in the oceans. However, great care must be taken when correlating carbonate chemistry with coccolithophore dispersal because this is by no means the only parameter controlling it. Physical (e.g. temperature), other chemical (e.g. nutrient concentrations), or ecological (e.g. grazing pressure) factors will under many if not most circumstances outweigh the influence of carbonate chemistry conditions, unless differences in the latter are extreme. We will therefore focus the discussion on those cases where differences in carbonate chemistry conditions are rather extreme – for example the comparison between the Mesozoic and the modern ocean.

Today, coccolithophores are present in all oceans and most marginal seas, including the semi-enclosed Mediterranean, Black and Caspian Sea, as well as the western but not the eastern part of the Baltic Sea (Kideys et al., 2005; Moore et al., 2012; Silkin et al., 2014; Tyrrell et al., 2008). The Black Sea has considerably higher total alkalinities than the global ocean, leading to high availability of HCO_3^- substrate and comparatively lower $[\text{H}^+]$ at atmosphere-equilibrated $p\text{CO}_2$ (Goyet et al., 1991). These should be particularly calcification-favorable carbonate chemistry conditions (Fig. 8). And indeed, the Black Sea frequently harbors extensive *E. huxleyi* blooms (Kopelevich et al., 2014), especially since diatom proliferation is limited by reduced silicate input as a consequence of the Danube River dam construction in the early 1970’s (Humborg et al., 1997).

Total alkalinity of the eastern Baltic Sea is much lower than the global ocean mean which results in calcite under-saturation during winter time (Tyrrell et al., 2008). This led Tyrrell et al., 2008 to suggest that one reason for the absence of coccolithophores in this region could be reoccurring corrosive conditions which the calcareous armor cannot fully resist. Our interpretations resemble those of Tyrrell et al. with the key difference that we argue from the perspective of CaCO_3 formation, not dissolution. According to our results, calcification would be comparatively energy-consuming in the Baltic proper (below the CBT) so that diatoms, using cheaper and in this region permanently available silicate (Sandén and Danielsson, 1995) to construct their armor, outcompete coccolithophores (Figs. 6 and 7).

Coccolithophores have their first appearance in the fossil record during the Upper Triassic (~225 million years ago; Bown et al., 2004) and diversify thereafter until the end of the Cretaceous (Martin, 1995). Carbonate chemistry reconstructions of these periods suggest generally higher surface ocean $p\text{CO}_2$ and lower pH than at present day (Zeebe, 2012). However, high- $p\text{CO}_2$ /low-pH

Table 4

Culture conditions for experiments with *E. huxleyi* strain NZEH, RCC1216, RCC1212, RCC1216, and RCC1238 shown in Fig. 5. The origin of each strain and the time of its isolation is given in Langer et al. (2009). pH_{NBS} and pH_{total} indicates that pH values were reported on the NBS and total scale, respectively. Continuous bubbling indicates that cultures were aerated with CO_2 gas mixtures during the whole experiment, while pre-inoculation bubbling denotes that aeration stopped when cells were inoculated. Acid-base addition at constant TA indicates that TA was re-adjusted with NaHCO_3 after acid and base additions to yield the same TA between treatments. Re-adjustment was omitted in “the acid-base constant DIC” approach. NSW = natural seawater. The arrows illustrate observed responses in calcification rates with \uparrow (increasing), \downarrow (decreasing), \leftrightarrow (constant), and \cap (optimum curve) found within the investigated pCO_2 range. Letters behind arrows express whether results were significant (a) or not (b) when a statistical analysis was reported by the authors.

Color code in Fig. 5	pCO_2 calculation based on:	CO_2 manipulation	Temperature ($^{\circ}\text{C}$)	Light intensity ($\mu\text{mol m}^{-2} \text{s}^{-1}$)	Light:dark cycle (h:h)	Salinity	Culture medium	Calcification response	Reference
<i>NZEH (variable experimental protocol and culture conditions, Fig. 5a)</i>									
Gray	TA, DIC	Continuous bubbling	19	150	12:12	34		\uparrow a	Iglesias-Rodriguez et al. (2008a,b)
Blue	TA, DIC	Continuous bubbling	19	80–120	12:12		NSW (English Channel)	\uparrow b	Jones et al. (2013) ^a
Green	TA, DIC	Continuous bubbling	19	80–120	12:12		NSW (English Channel)	\uparrow b	Jones et al. (2013) ^b
Red	pH_{total} , TA	Continuous bubbling	20	150	24:0		NSW (Gulf stream)	\downarrow b	Shi et al. (2009)
Orange	pH_{total} , TA	Acid-base constant TA	20	150	24:0		NSW (Gulf stream)	\uparrow b	Shi et al. (2009)
Yellow	pH_{NBS} , DIC	Pre-inoculation bubbling	15	170	16:8	32.4	NSW (North Sea)	\downarrow a	Hoppe et al. (2011)
Turquoise	pH_{NBS} , DIC	Acid-base constant DIC	15	170	16:8	32.4	NSW (North Sea)	\downarrow a	Hoppe et al. (2011)
Pink	pH_{NBS} , DIC	Continuous bubbling	15	170	16:8	32.4	NSW (North Sea)	\cap a	Hoppe et al. (2011)
<i>RCC1216 (variable experimental protocol and culture conditions, Fig. 5b)</i>									
Gray	pH_{total} , TA	Pre-inoculation bubbling	17	150	14:10	38		\uparrow b	Richier et al. (2011)
Blue	TA, DIC	Acid-base constant DIC	17	400	16:8	32	NSW (North Sea)	\downarrow	Langer et al. (2009)
Green	pH_{NBS} , TA	Continuous bubbling	15	50	16:8	32	NSW (North Sea)	\downarrow a	Rokitta and Rost (2012)
Red	pH_{NBS} , TA	Continuous bubbling	15	300	16:8	32	NSW (North Sea)	\downarrow b	Rokitta and Rost (2012)
Orange	pH_{NBS} , TA	Continuous bubbling	15	300	16:8	32.4	NSW (North Sea)	\downarrow a	Kottmeier et al. (2014)
<i>Strain comparison under identical experimental protocol and culture conditions, Fig. 5c</i>									
Gray triangle (RCC1238), gray square (RCC1212)	TA, DIC	Acid-base constant DIC	20	400	16:8	32	NSW (North Sea)	\leftrightarrow , (1238) \downarrow (1212)	(Langer et al., 2009)
Blue triangle (RCC1216), blue square (RCC1256)	TA, DIC	Acid-base constant DIC	17	400	16:8	32	NSW (North Sea)	\downarrow , (1216) \cap (1256)	(Langer et al., 2009)
Red triangle (RCC1256), red square (NZEH)	pH_{NBS} , DIC	Acid-base constant DIC	15	170	16:8	32.4	NSW (North Sea)	\downarrow a, (1256) \downarrow a, (NZEH)	(Hoppe et al., 2011)

^a After 6–7 days of incubation.

^b After 8–10 days of incubation.

conditions were probably accompanied with elevated HCO_3^- , since rock weathering and dissolution of deep-ocean CaCO_3 sediments enhanced the oceans' alkalinity (Hönisch et al., 2012; Ridgwell and Zeebe, 2005; Zeebe, 2012). Thus, unfavorably high $[\text{H}^+]$ might have been compensated by high substrate availability thereby creating carbonate chemistry conditions which supported high calcification rates. This could be another chemical prerequisite (next to e.g. high $[\text{Ca}^{2+}]$; Stanley and Hardie, 1998) of why coccolithophores were able to constitute such a prominent component of the mid- to late-Mesozoic phytoplankton community.

CO_2 is currently released to the atmosphere at a rate unparalleled for at least the last 300 million years (Hönisch et al., 2012). The fast pace limits prompt dampening of ocean acidification by geochemical buffering like weathering and carbonate sediment dissolution (Ridgwell, 2005; Zeebe, 2012). These will only come into play on millennial time-scales leaving anthropogenic ocean acidification as a short pulse (~ 10 – 20 kyears; Archer et al., 2009; Ridgwell and Hargreaves, 2007) of strongly increased $[\text{H}^+]$ and only slightly increased $[\text{HCO}_3^-]$ (Hönisch et al., 2012; Zeebe, 2012). If coccolithophorid calcification remains unable to fully adapt to

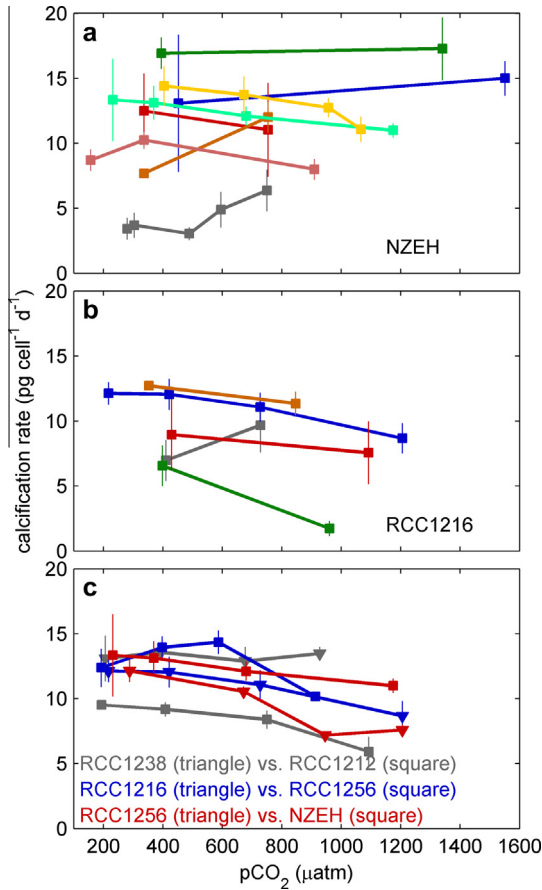


Fig. 5. Response in calcification rates of different *E. huxleyi* strains to increasing $p\text{CO}_2$. Panel (a) and (b) show the variability in the response of strain NZEH and RCC1216 when grown under different culture conditions and applying different experimental protocols. Panel (c) shows the variability in the response when different strains were grown under identical culture conditions and applying an identical experimental protocol. Comparing panels (a, b) with (c) suggests that the variability caused by inconsistent culture conditions and experimental protocols is at least equally important as the genetic variability among strains. Color coding and details on culture conditions for each experiment are given in Table 4. (For interpretation of the references to color in this figure legend, the reader is referred to the web version of this article.)

the H^+ pulse, other functional groups whose shell construction is not handicapped may become more competitive during this time thereby further narrowing the realized niche of calcification by elevating the CBT (Fig. 6).

Tides may turn, however, when the acidification pulse starts to retreat (5–10 kyears in the future; Archer et al., 2009; Ridgwell and Hargreaves, 2007). When deep-ocean CaCO_3 sediment dissolution and terrestrial weathering kick in and release significant amounts of carbonate alkalinity ($[\text{HCO}_3^-] + 2[\text{CO}_3^{2-}]$) into the oceans, H^+ concentrations slowly decline while HCO_3^- increases. Simultaneously, increased alkalinity causes CO_2 under-saturation of the surface oceans leading to in-gassing of additional amounts of atmospheric CO_2 . Model simulations consistently show that the oceans will contain more $\text{HCO}_3^- \sim 50,000$ years into the future than at present while $[\text{H}^+]$ will be similarly low (Archer et al., 2009; Ridgwell and Hargreaves, 2007) with the degree of long-term carbonation positively scaling with the amount of anthropogenic CO_2 that will be released into the atmosphere (Hönisch et al., 2012; Ridgwell and Hargreaves, 2007; Zeebe, 2012). These relatively high-substrate/low-inhibitor carbonate chemistry conditions of the far

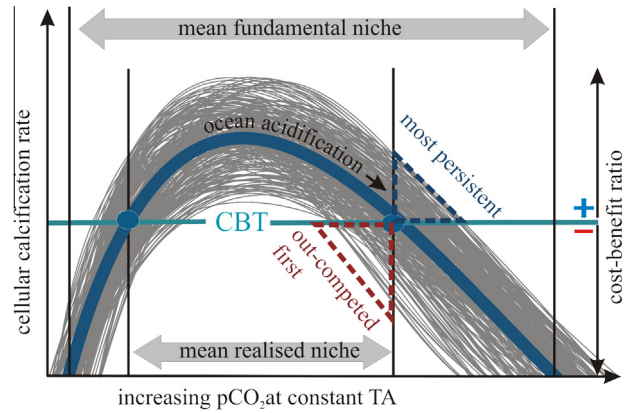


Fig. 6. Conceptual figure on the response of all coccolithophore genotypes (thin grey lines with the thick blue line being the mean) to a large $p\text{CO}_2$ gradient at constant total alkalinity. Complete optimum curves represent the fundamental niches of calcification and therefore the carbonate chemistry conditions where calcification is physiologically possible. The horizontal turquoise line denotes the ‘cost benefit threshold’ (CBT) above which the benefits of being able to calcify exceed the associated costs. The CBT therefore constrains the realized niche of calcification where this trait promotes the competitiveness of coccolithophores relative to other groups. The points where optimum curves cross the CBT can be considered as tipping points below which the individual genotype is out-competed because costs for calcification exceed its benefit and the competitive advantage is lost. Red-framed genotypes would be the first to fall below the CBT in an ocean acidification scenario while blue framed ones are less sensitive to increasing $[\text{H}^+]$ and remain in the realized niche longest. This illustrates how selection on standing genetic diversity is implemented in this concept.

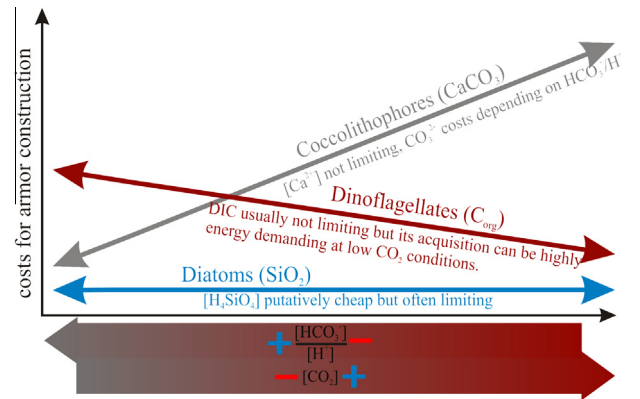


Fig. 7. Illustration of a thought experiment on the energetic effort for armor construction in three major shell-forming phytoplankton taxa as a function of carbonate chemistry conditions. The frustule (diatom shell) is considered the most inexpensive armor under all circumstances because diatoms typically outcompete all other groups when silicate is available. The coccosphere is relatively inexpensive under sufficient $[\text{CO}_2]$, high $[\text{HCO}_3^-]$, and low $[\text{H}^+]$ because substrate is saturating and protons are easily released into seawater (Taylor et al., 2011). In contrast, the construction of thecal elements, which are organic (cellulose) plates that constitute the dinoflagellate shell, should rather be favored at high H^+ concentrations because these usually coincide with high $[\text{CO}_2]$. Under these conditions dinoflagellates could down-regulate the energy-consuming operation of carbon concentrating mechanisms to fuel the production of organic source material for their shell. Therefore, a shift in carbonate chemistry conditions toward high $[\text{CO}_2]$ may promote their competitiveness relative to coccolithophores. It must be kept in mind, however, that such a hypothetical gain in competitiveness due to altered carbonate chemistry conditions would not automatically lead to dinoflagellate dominance because a huge number of factors other than carbonate chemistry have an influence on species composition as well.

future may facilitate coccolithophorid calcification after the inhibiting effect of high H^+ concentrations due to present and near future ocean acidification has disappeared.

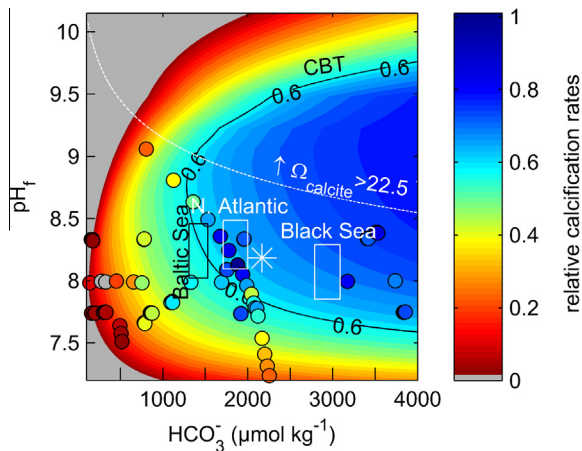


Fig. 8. Same data as in Fig. 2a but plotted in a pH vs. $[\text{HCO}_3^-]$ matrix. The dotted white line indicates the threshold above which calcite starts to precipitate inorganically (Morse et al., 2003). The black line indicates the CBT (arbitrary value of 0.6) and therefore a possible threshold above which the benefits of calcification in a competitive environment exceed its costs (see Fig. 6). The black and white boxes indicate surface water carbonate chemistry conditions (0–45 m) of certain ocean basins (Data taken from Goyet et al., 1991; Key et al., 2004; Tyrrell et al., 2008). The white asterisk exemplifies potential mean surface ocean carbonate chemistry conditions (upper 87 m) in 50,000 years from now, assuming the IPCC “business-as-usual” A2 emission scenario until the year 2100 followed by a linear decrease of CO_2 emissions until the year 2300. Calculations were done with the GENIE-1 earth system model including sediment dissolution and terrestrial weathering (Ridgwell et al., 2007) set up as in (Archer et al., 2009). Note that smaller or larger CO_2 perturbations than simulated here would lead to less or more pronounced $[\text{HCO}_3^-]$ increases in the far future (Ridgwell and Hargreaves, 2007).

Author contributions

Designed research: LTB, KGS, MG.
 Performed research: LTB, MG, LF.
 Contributed new reagents or analytic tools: KGS, UR, MG.
 Analyzed data: LTB, KGS, MG, LF.
 Wrote the paper: LTB, KGS, UR.

Acknowledgments

L.T. Bach would like to thank Kai Lohbeck and Luke Mackinder for the frequent and valuable discussions and Andy Ridgwell for his calculations with the GENIE-1 model. Furthermore, we are grateful to Lena Holtz and two anonymous reviewers for their valuable comments. This study was funded by the Federal Ministry of Education and Research (BMBF) in the framework of the Biological Impacts of Ocean Acidification II (BIOACID II) project (W.P. 1.3).

Appendix A. Supplementary material

Supplementary data associated with this article can be found, in the online version, at <http://dx.doi.org/10.1016/j.pcean.2015.04.012>.

References

Archer, D., Eby, M., Brovkin, V., Ridgwell, A., Cao, L., Mikolajewicz, U., Caldeira, K., Matsumoto, K., Munhoven, G., Montenegro, A., Tokos, K., 2009. Atmospheric lifetime of fossil fuel carbon dioxide. *Annual Review of Earth and Planetary Sciences* 37, 117–134. <http://dx.doi.org/10.1146/annurev.earth.031208.100206>.
 Armstrong, R.A., Lee, C., Hedges, J.L., Honjo, S., Wakeham, S.G., 2002. A new, mechanistic model for organic carbon fluxes in the ocean based on the quantitative association of POC with ballast minerals. *Deep Sea Research Part II: Topical Studies in Oceanography* 49, 219–236.

Bach, L.T., Riebesell, U., Schulz, K.G., 2011. Distinguishing between the effects of ocean acidification and ocean carbonation in the coccolithophore *Emiliana huxleyi*. *Limnology and Oceanography* 56, 2040–2050. <http://dx.doi.org/10.4319/lno.2011.56.6.2040>.
 Bach, L.T., Bauke, C., Meier, K.J.S., Riebesell, U., Schulz, K.G., 2012. Influence of changing carbonate chemistry on morphology and weight of coccoliths formed by *Emiliana huxleyi*. *Biogeosciences* 9, 3449–3463. <http://dx.doi.org/10.5194/bg-9-3449-2012>.
 Bach, L.T., Mackinder, L.C.M., Schulz, K.G., Wheeler, G., Schroeder, D.C., Brownlee, C., Riebesell, U., 2013. Dissecting the impact of CO_2 and pH on the mechanisms of photosynthesis and calcification in the coccolithophore *Emiliana huxleyi*. *New Phytologist* 199, 121–134. <http://dx.doi.org/10.1111/nph.12225>.
 Beaufort, L., Probert, I., de Garidel-Thoron, T., Bendif, E.M., Ruiz-Pino, D., Metzl, N., Goyet, C., Buchet, N., Coupel, P., Grelaud, M., Rost, B., Rickaby, R.E.M., de Vargas, C., 2011. Sensitivity of coccolithophores to carbonate chemistry and ocean acidification. *Nature* 476, 80–83. <http://dx.doi.org/10.1038/nature10295>.
 Benner, I., Diner, R.E., Levebvre, S.C., Li, D., Komada, T., Carpenter, E.J., Stillman, J.H., 2013. *Emiliana huxleyi* increases calcification but not expression of calcification-related genes in long-term exposure to elevated temperature and pCO_2 . *Proceedings of the Royal Society B: Biological Sciences* 368, 20130049.
 Bown, P.R., Lees, J.A., Young, J.R., 2004. Calcareous nannoplankton evolution and diversity through time. In: Thierstein, H.-R., Young, J.R. (Eds.), *In Coccolithophores: From Molecular Processes to Global Impact*. Springer, Heidelberg, pp. 481–508.
 Broecker, W., Clark, E., 2009. Ratio of coccolith CaCO_3 to foraminifera CaCO_3 in late Holocene deep sea sediments. *Paleoceanography* 24, PA3205. <http://dx.doi.org/10.1029/2009PA001731>.
 Brownlee, C., Taylor, A.R., 2004. Calcification in coccolithophores: a cellular perspective. In: Thierstein, H.R., Young, J.R. (Eds.), *Coccolithophores: From Molecular Processes to Global Impact*. Springer, Heidelberg, pp. 31–49.
 Buitenhuis, E.T., de Baar, H.J.W., Veldhuis, M.J.W., 1999. Photosynthesis and calcification by *Emiliana huxleyi* (Prymnesiophyceae) as a function of inorganic carbon species. *Journal of Phycology* 35, 949–959. <http://dx.doi.org/10.1046/j.1529-8817.1999.3550949.x>.
 Collins, S., Rost, B., Rynearson, T.A., 2014. Evolutionary potential of marine phytoplankton under ocean acidification. *Evolutionary Applications* 7, 140–155. <http://dx.doi.org/10.1111/eva.12120>.
 De Bodt, C., Van Oostende, N., Harlay, J., Sabbe, K., Chou, L., 2010. Individual and interacting effects of pCO_2 and temperature on *Emiliana huxleyi* calcification: study of the calcite production, the coccolith morphology and the coccosphere size. *Biogeosciences* 7, 1401–1412. <http://dx.doi.org/10.5194/bg-7-1401-2010>.
 Dickson, A.G., Sabine, C.L., Christian, J.R., 2007. *Guide to Best Practices for Ocean CO_2 Measurements*, PICES Spec. ed. PICES, Sidney.
 Erba, E., 2006. The first 150 million years history of calcareous nannoplankton: biosphere-geosphere interactions. *Palaeogeography, Palaeoclimatology, Palaeoecology* 232, 237–250. <http://dx.doi.org/10.1016/j.palaeo.2005.09.013>.
 Erba, E., Tremolada, F., 2004. Nannofossil carbonate fluxes during the Early Cretaceous: Phytoplankton response to nitrification episodes, atmospheric CO_2 , and anoxia. *Paleoceanography* 19, 1–18. <http://dx.doi.org/10.1029/2003PA000884>.
 Feng, Y., Warner, M.E., Zhang, Y., Sun, J., Fu, F.-X., Rose, J.M., Hutchins, D.A., 2008. Interactive effects of increased pCO_2 , temperature and irradiance on the marine coccolithophore *Emiliana huxleyi* (Prymnesiophyceae). *European Journal of Phycology* 43, 87–98. <http://dx.doi.org/10.1080/09670260701664674>.
 Flynn, K.J., Blackford, J.C., Baird, M.E., Raven, J.A., Clark, D.R., Beardall, J., Brownlee, C., Fabian, H., Wheeler, G.L., 2012. Changes in pH at the exterior surface of plankton with ocean acidification. *Nature Climate Change* 2, 510–513.
 Frankignoulle, M., Canon, C., Gattuso, J.-P., 1994. Marine calcification as a source of carbon dioxide: positive feedback of increasing atmospheric CO_2 . *Limnology and Oceanography* 39, 458–462.
 Fu, F.X., Zhang, Y., Warner, M.E., Feng, Y., Sun, J., Hutchins, D.A., 2008. A comparison of future increased CO_2 and temperature effects on sympatric *Heterosigma akashiwo* and *Prorocentrum minimum*. *Harmful Algae* 7, 76–90. <http://dx.doi.org/10.1016/j.hal.2007.05.006>.
 Gao, K., Ruan, Z., Villafane, V.E., Gattuso, J.-P., Helbling, E.W., 2009. Ocean acidification exacerbates the effect of UV radiation on the calcifying phytoplankton *Emiliana huxleyi*. *Limnology and Oceanography* 54, 1855–1862.
 Goyet, C., Bradshaw, A.L., Brewer, P.G., 1991. The carbonate system in the Black Sea. *Deep Sea Research Part A: Oceanographic Research Papers* 38, S1049–S1068. [http://dx.doi.org/10.1016/S0198-0149\(10\)80023-8](http://dx.doi.org/10.1016/S0198-0149(10)80023-8).
 Guillard, R.R.L., Rytter, J.H., 1962. Studies of marine planktonic diatoms: I. *Cyclotella nana* Husted, and *Detonula confervacea* (Cleve) gran. *Canadian Journal of Microbiology* 8, 229–239.
 Hamm, C., Smetacek, V., 2007. *Armor: Why, when, and how*. In: Falkowski, P.G., Knoll, A.H. (Eds.), *Evolution of Phytoplankton*. Elsevier, Boston, pp. 311–332.
 Holtz, L.-M., Wolf-Gladrow, D., Thoms, S., 2015. Numerical cell model investigating cellular carbon fluxes in *Emiliana huxleyi*. *Journal of Theoretical Biology* 364, 305–315. <http://dx.doi.org/10.1016/j.jtbi.2014.08.040>.
 Hönisch, B., Ridgwell, A., Schmidt, D.N., Thomas, E., Gibbs, S.J., Sluijs, A., Zeebe, R., Kump, L., Martindale, R.C., Greene, S.E., Kiessling, W., Ries, J., Zachos, J.C., Royer, D.L., Barker, S., Marchitto, T.M., Moyer, R., Pelejero, C., Ziveri, P., Foster, G.L., Williams, B., 2012. The geological record of ocean acidification. *Science* 335, 1058–1063. <http://dx.doi.org/10.1126/science.1208277>.
 Hopkinson, B.M., Dupont, C.L., Allen, A.E., Morel, F.M.M., 2011. Efficiency of the CO_2 -concentrating mechanism of diatoms. *Proceedings of the National Academy of Sciences* 108, 1058–1063. <http://dx.doi.org/10.1073/pnas.1011263108>.

- Sciences of the United States of America 108, 3830–3837. <http://dx.doi.org/10.1073/pnas.1018062108>.
- Hoppe, C.J.M., Langer, G., Rost, B., 2011. *Emiliania huxleyi* shows identical responses to elevated pCO₂ in TA and DIC manipulations. *Journal of Experimental Marine Biology and Ecology* 406, 54–62. <http://dx.doi.org/10.1016/j.jembe.2011.06.008>.
- Humborg, C., Ittekkot, V., Cociasu, A., von Bodungen, B., 1997. Effect of Danube River dam on Black Sea biogeochemistry and ecosystem structure. *Nature* 386, 385–388.
- Hutchinson, G.E., 1957. Concluding remarks. In: *Concluding Remarks: Cold Spring Harbor Symposium on Quantitative Biology*, pp. 415–427.
- Iglesias-Rodriguez, M.D., Buitenhuis, E.T., Raven, J.A., Schofield, O., Poulton, A.J., Gibbs, S., Halloran, P.R., De Baar, H.J.W., 2008a. Response to Comment on “Phytoplankton Calcification in a High-CO₂ World”, 322, 1466c.
- Iglesias-Rodriguez, M.D., Halloran, P.R., Rickaby, R.E.M., Hall, I.R., Colmenero-Hidalgo, E., Gittins, J.R., Green, D.R.H., Tyrrell, T., Gibbs, S.J., von Dassow, P., Rehm, E., Armbrust, E.V., Boessenkool, K.P., 2008b. Phytoplankton calcification in a high-CO₂ world. *Science* 320, 336–340. <http://dx.doi.org/10.1126/science.1154122>.
- Jin, P., Gao, K., Beardall, J., 2013. Evolutionary responses of a coccolithophorid *Gephyrocapsa oceanica* to ocean acidification. *Evolution (N.Y.)* 67, 1869–1878. <http://dx.doi.org/10.1111/evo.12112>.
- Jones, B.M., Iglesias-Rodriguez, M.D., Skipp, P.J., Edwards, R.J., Greaves, M.J., Young, J.R., Elderfield, H., O'Connor, C.D., 2013. Responses of the *Emiliania huxleyi* proteome to ocean acidification. *PLoS ONE* 8, e61868. <http://dx.doi.org/10.1371/journal.pone.0061868>.
- Kearney, M., Porter, W., 2009. Mechanistic niche modelling: combining physiological and spatial data to predict species' ranges. *Ecology Letters* 12, 334–350. <http://dx.doi.org/10.1111/j.1461-0248.2008.01277.x>.
- Kester, D.R., Duedall, I.W., Connors, D.N., Pytkowicz, R.M., 1967. Preparation of artificial seawater. *Limnology and Oceanography* 12, 176–179.
- Key, R.M., Kozyr, A., Sabine, C.L., Lee, K., Wanninkhof, R., Bullister, J.L., Feely, R.A., Millero, F.J., Mordy, C., Peng, T.-H., 2004. A global ocean carbon climatology: Results from Global Data Analysis Project (GLODAP). *Global Biogeochemical Cycles* 18, GB4031. <http://dx.doi.org/10.1029/2004GB002247>.
- Kideys, A.E., Soydemir, N., Eker, E., Vladymyrov, V., Soloviev, D., Melin, F., 2005. Phytoplankton distribution in the Caspian Sea during March 2001. *Hydrobiologia* 543, 159–168. <http://dx.doi.org/10.1007/s10750-004-6953-x>.
- Kopelevich, O., Burenkov, V., Sheberstov, S., Vazyulya, S., Kravchishina, M., Pautova, L., Silkin, V., Artemiev, V., Grigoriev, A., 2014. Satellite monitoring of coccolithophore blooms in the Black Sea from ocean color data. *Remote Sensing of Environment* 146, 113–123. <http://dx.doi.org/10.1016/j.rse.2013.09.009>.
- Kottmeier, D.M., Rokitta, S.D., Tortell, P.D., Rost, B., 2014. Strong shift from HCO₃⁻ to CO₂ uptake in *Emiliania huxleyi* with acidification: new approach unravels acclimation versus short-term pH effects. *Photosynthesis Research*. <http://dx.doi.org/10.1007/s11120-014-9984-9>.
- Langer, G., Geisen, M., Baumann, K.-H., Kläs, J., Riebesell, U., Thoms, S., Young, J.R., 2006. Species-specific responses of calcifying algae to changing seawater carbonate chemistry. *Geochemistry, Geophysics, Geosystems* 7. <http://dx.doi.org/10.1029/2005GC001227>.
- Langer, G., Nehrke, G., Probert, I., Ly, J., Ziveri, P., 2009. Strain-specific responses of *Emiliania huxleyi* to changing seawater carbonate chemistry. *Biogeosciences* 6, 2637–2646. <http://dx.doi.org/10.5194/bg-6-2637-2009>.
- Lewis, E., Wallace, D.W.R., 1998. Program Developed for CO₂ System Calculations.
- Liu, H., Aris-Brosou, S., Probert, I., de Vargas, C., 2010. A time line of the environmental genetics of the haptophytes. *Molecular Biology and Evolution* 27, 161–176. <http://dx.doi.org/10.1093/molbev/msp222>.
- Lohbeck, K.T., Riebesell, U., Reusch, T.B.H., 2012. Adaptive evolution of a key phytoplankton species to ocean acidification. *Nature Geoscience* 5, 346–351. <http://dx.doi.org/10.1038/ngeo1441>.
- Lohbeck, K.T., Riebesell, U., Reusch, T.B.H., 2014. Gene expression changes in the coccolithophore *Emiliania huxleyi* after 500 generations of selection to ocean acidification. *Proceedings of the Royal Society B: Biological Sciences* 281, 1–7.
- Martin, R.E., 1995. Cyclic and secular variation in microfossil biomineralization: clues to the biogeochemical evolution of Phanerozoic oceans. *Global and Planetary Change* 11, 1–23.
- Moore, T.S., Dowell, M.D., Franz, B.A., 2012. Detection of coccolithophore blooms in ocean color satellite imagery: a generalized approach for use with multiple sensors. *Remote Sensing of Environment* 117, 249–263. <http://dx.doi.org/10.1016/j.rse.2011.10.001>.
- Morse, J.W., Gledhill, D.K., Millero, F.J., 2003. CaCO₃ precipitation kinetics in waters from the great Bahama bank: implications for the relationship between bank hydrochemistry and whittings. *Geochimica et Cosmochimica Acta* 67, 2819–2826. [http://dx.doi.org/10.1016/S0016-7037\(03\)00103-0](http://dx.doi.org/10.1016/S0016-7037(03)00103-0).
- Muller, E.B., Nisbet, R.M., 2014. Dynamic energy budget modeling reveals the potential of future growth and calcification for the coccolithophore *Emiliania huxleyi* in an acidified ocean. *Global Change Biology* 20, 2031–2038. <http://dx.doi.org/10.1111/gcb.12547>.
- Müller, M.N., Schulz, K.G., Riebesell, U., 2010. Effects of long-term high CO₂ exposure on two species of coccolithophores. *Biogeosciences* 7, 1109–1116. <http://dx.doi.org/10.5194/bg-7-1109-2010>.
- Nimer, N.A., Merrett, M.J., 1993. Calcification rate in *Emiliania huxleyi* Lohmann in response to light, nitrate and availability of inorganic carbon. *New Phytologist* 123, 673–677. <http://dx.doi.org/10.1111/j.1469-8137.1993.tb03776.x>.
- Paasche, E., 1964. A tracer study of the inorganic carbon uptake during coccolith formation and photosynthesis in the coccolithophorid *Coccolithus huxleyi*. *Physiologia Plantarum Supplementum* 3, 1–84.
- Pörtner, H.-O., Farrell, A.P., 2008. Physiology and climate change. *Science* 322, 690–692. <http://dx.doi.org/10.1126/science.1163156>.
- Poulton, A.J., Adey, T.R., Balch, W.M., Holligan, P.M., 2007. Relating coccolithophore calcification rates to phytoplankton community dynamics: regional differences and implications for carbon export. *Deep Sea Research Part II: Topical Studies in Oceanography* 54, 538–557. <http://dx.doi.org/10.1016/j.dsr2.2006.12.003>.
- Read, B.A., Kegel, J., Klute, M.J., Kuo, A., Lefebvre, S.C., Maumus, F., Mayer, C., Miller, J., Monier, A., Salamov, A., Young, J., Aguilar, M., Claverie, J.-M., Frickenhaus, S., Gonzalez, K., Herman, E.K., Lin, Y.-C., Napier, J., Ogata, H., Sarno, A.F., Shmutz, J., Schroeder, D., de Vargas, C., Verret, F., von Dassow, P., Valentin, K., Van de Peer, Y., Wheeler, G., Dacks, J.B., Delwiche, C.F., Dyhrman, S.T., Glöckner, G., John, U., Richards, T., Worden, A.Z., Zhang, X., Grigoriev, I.V., 2013. Pan genome of the phytoplankton *Emiliania* underpins its global distribution. *Nature* 499, 209–213. <http://dx.doi.org/10.1038/nature12221>.
- Reinfelder, J.R., 2011. Carbon concentrating mechanisms in eukaryotic marine phytoplankton. *Annual Review of Marine Science* 3, 291–315. <http://dx.doi.org/10.1146/annurev-marine-120709-142720>.
- Richier, S., Fiorini, S., Kerros, M.-E., von Dassow, P., Gattuso, J.-P., 2011. Response of the calcifying coccolithophore *Emiliania huxleyi* to low pH/high pCO₂: from physiology to molecular level. *Marine Biology* 158, 551–560. <http://dx.doi.org/10.1007/s00227-010-1580-8>.
- Rickaby, R.E.M., Henderiks, J., Young, J.N., 2010. Perturbing phytoplankton: response and isotopic fractionation with changing carbonate chemistry in two coccolithophore species. *Climate of the Past* 6, 771–785. <http://dx.doi.org/10.5194/cp-6-771-2010>.
- Ridgwell, A., 2005. A Mid Mesozoic Revolution in the regulation of ocean chemistry. *Marine Geology* 217, 339–357. <http://dx.doi.org/10.1016/j.margeo.2004.10.036>.
- Ridgwell, A., Hargreaves, J.C., 2007. Regulation of atmospheric CO₂ by deep-sea sediments in an Earth system model. *Global Biogeochemical Cycles* 21. <http://dx.doi.org/10.1029/2006GB002764>, n/a–n/a.
- Ridgwell, A., Zeebe, R., 2005. The role of the global carbonate cycle in the regulation and evolution of the Earth system. *Earth and Planetary Science Letters* 234, 299–315. <http://dx.doi.org/10.1016/j.epsl.2005.03.006>.
- Ridgwell, A., Hargreaves, J.C., Edwards, N.R., Annan, J.D., Lenton, T.M., Marsh, R., Yool, A., Watson, A., 2007. Marine geochemical data assimilation in an efficient Earth System Model of global biogeochemical cycling. *Biogeosciences* 4, 87–104. <http://dx.doi.org/10.5194/bg-4-87-2007>.
- Riebesell, U., Tortell, P.D., 2011. Effects of ocean acidification on pelagic organisms and ecosystems. In: Gattuso, J.-P., Hansson, L. (Eds.), *Ocean Acidification*. Oxford University Press, Oxford, pp. 99–121.
- Riebesell, U., Zondervan, I., Rost, B., Tortell, P.D., Zeebe, R.E., Morel, F.M.M., 2000. Reduced calcification of marine plankton in response to increased atmospheric CO₂. *Nature* 407, 364–367.
- Riebesell, U., Bellerby, R.G.J., Engel, A., Fabry, V.J., Hutchins, D.A., Reusch, T.B.H., Schulz, K.G., Morel, F.M.M., 2008. Comment on “Phytoplankton calcification in a high-CO₂ world”. *Science* 322, 1466b. <http://dx.doi.org/10.1126/science.1161096>.
- Riebesell, U., Körtzinger, A., Oschlies, A., 2009. Sensitivities of marine carbon fluxes to ocean change. *Proceedings of the National Academy of Sciences of the United States of America* 106, 20602–20609. <http://dx.doi.org/10.1073/pnas.0813291106>.
- Rokitta, S.D., Rost, B., 2012. Effects of CO₂ and their modulation by light in the life-cycle stages of the coccolithophore *Emiliania huxleyi*. *Limnology and Oceanography* 57, 607–618. <http://dx.doi.org/10.4319/lo.2012.57.2.0607>.
- Rokitta, S.D., John, U., Rost, B., 2012. Ocean acidification affects redox-balance and ion-homeostasis in the life-cycle stages of *Emiliania huxleyi*. *PLoS ONE* 7, e52212. <http://dx.doi.org/10.1371/journal.pone.0052212>.
- Rost, B., Riebesell, U., Burkhardt, S., Sültemeyer, D., 2003. Carbon acquisition of bloom-forming marine phytoplankton. *Limnology and Oceanography* 48, 55–67.
- Rost, B., Riebesell, U., Sültemeyer, D., 2006. Carbon acquisition of marine phytoplankton: Effect of photoperiod length. *Limnology and Oceanography* 51, 12–20.
- Roy, R.N., Roy, L.N., Vogel, K.M., Porter-Moore, C., Pearson, T., Good, C.E., Millero, F.J., Campbell, D.M., 1993. The dissociation constants of carbonic acid in seawater at salinities 5 to 45 and temperatures 0 to 45 °C. *Marine Chemistry* 44, 249–267. [http://dx.doi.org/10.1016/0304-4203\(93\)90207-5](http://dx.doi.org/10.1016/0304-4203(93)90207-5).
- Sandén, P., Danielsson, A., 1995. Spatial properties of nutrient concentrations in the Baltic Sea. *Environmental Monitoring and Assessment* 34, 289–307.
- Schulz, K.G., Rost, B., Burkhardt, S., Riebesell, U., Thoms, S., Wolf-Gladrow, D., 2007. The effect of iron availability on the regulation of inorganic carbon acquisition in the coccolithophore *Emiliania huxleyi* and the significance of cellular compartmentation for stable carbon isotope fractionation. *Geochimica et Cosmochimica Acta* 71, 5301–5312. <http://dx.doi.org/10.1016/j.gca.2007.09.012>.
- Sciandra, A., Harlay, J., Lefèvre, D., Lemée, R., Rimmelin, P., Denis, M., Gattuso, J.-P., 2003. Response of coccolithophorid *Emiliania huxleyi* to elevated partial pressure of CO₂ under nitrogen limitation. *Marine Ecology Progress Series* 261, 111–122. <http://dx.doi.org/10.3354/meps261111>.
- Sekino, K., Shiraiwa, Y., 1994. Accumulation and utilization of dissolved inorganic carbon by a marine unicellular coccolithophorid, *Emiliania huxleyi*. *Plant and Cell Physiology* 35, 353–361.

- Sett, S., Bach, L.T., Schulz, K.G., Koch-Klavnsen, S., Lebrato, M., Riebesell, U., 2014. Temperature modulates coccolithophorid sensitivity of growth, photosynthesis and calcification to increasing seawater pCO₂. PLoS ONE 9, e88308. <http://dx.doi.org/10.1371/journal.pone.0088308>.
- Shi, D., Xu, Y., Morel, F.M.M., 2009. Effects of the pH/pCO₂ control method on medium chemistry and phytoplankton growth. Biogeosciences 6, 1199–1207. <http://dx.doi.org/10.5194/bg-6-1199-2009>.
- Silkin, V.A., Pautova, L.A., Pakhomova, S.V., Lifanchuk, A.V., Yakushev, E.V., Chasovnikov, V.K., 2014. Environmental control on phytoplankton community structure in the NE Black Sea. Journal of Experimental Marine Biology and Ecology 461, 267–274. <http://dx.doi.org/10.1016/j.jembe.2014.08.009>.
- Smith, H.E.K., Tyrrell, T., Charalampopoulou, A., Dumousseaud, C., Legge, O.J., Birchenough, S., Pettit, L.R., Garley, R., Hartman, S.E., Hartman, M.C., Sagoo, N., Daniels, C.J., Achterberg, E.P., Hydes, D.J., 2012. Predominance of heavily calcified coccolithophores at low CaCO₃ saturation during winter in the Bay of Biscay. Proceedings of the National Academy of Sciences United States 109, 8845–8849. <http://dx.doi.org/10.1073/pnas.1117508109>.
- Stanley, S.M., Hardie, L.A., 1998. Secular oscillations in the carbonate mineralogy of reef-building and sediment-producing organisms driven by tectonically forced shifts in seawater chemistry. Palaeogeography, Palaeoclimatology, Palaeoecology 144, 3–19.
- Suffrian, K., Schulz, K.G., Gutowska, M.A., Riebesell, U., Bleich, M., 2011. Cellular pH measurements in *Emiliania huxleyi* reveal pronounced membrane proton permeability. New Phytologist 190, 595–608. <http://dx.doi.org/10.1111/j.1469-8137.2010.03633.x>.
- Taylor, A.R., Chrachri, A., Wheeler, G., Goddard, H., Brownlee, C., 2011. A voltage-gated H⁺ channel underlying pH homeostasis in calcifying coccolithophores. PLoS Biology 9, e1001085. <http://dx.doi.org/10.1371/journal.pbio.1001085>.
- Taylor, A.R., Brownlee, C., Wheeler, G.L., 2012. Proton channels in algae: reasons to be excited. Trends in Plant Science 17, 675–684. <http://dx.doi.org/10.1016/j.tplants.2012.06.009>.
- Tortell, P.D., 2000. Evolutionary and ecological perspectives on carbon acquisition in phytoplankton. Limnology and Oceanography 45, 744–750.
- Tyrrell, T., Holligan, P.M., Mobley, C.D., 1999. Optical impacts of oceanic coccolithophore blooms. Journal of Geophysical Research 104, 3223–3241. <http://dx.doi.org/10.1029/1998JC900052>.
- Tyrrell, T., Schneider, B., Charalampopoulou, A., Riebesell, U., 2008. Coccolithophores and calcite saturation state in the Baltic and Black Seas. Biogeosciences 5, 485–494. <http://dx.doi.org/10.5194/bg-5-485-2008>.
- Van de Waal, D.B., John, U., Ziveri, P., Reichart, G.-J., Hoins, M., Sluijs, A., Rost, B., 2013. Ocean acidification reduces growth and calcification in a marine dinoflagellate. PLoS ONE 8, e65987. <http://dx.doi.org/10.1371/journal.pone.0065987>.
- Wolf-Gladrow, D., Riebesell, U., 1997. Diffusion and reactions in the vicinity of plankton: a refined model for inorganic carbon transport. Marine Chemistry 59, 17–34. [http://dx.doi.org/10.1016/S0304-4203\(97\)00069-8](http://dx.doi.org/10.1016/S0304-4203(97)00069-8).
- Zeebe, R.E., 2012. History of seawater carbonate chemistry, atmospheric CO₂, and ocean acidification. Annual Review of Earth and Planetary Sciences 40, 141–165. <http://dx.doi.org/10.1146/annurev-earth-042711-105521>.
- Zeebe, R.E., Wolf-Gladrow, D.A., 2001. CO₂ in Seawater: Equilibrium, Kinetics, Isotopes. Elsevier O. ed. Elsevier, Amsterdam.